Biogeosciences Discuss., 8, 7257–7312, 2011
www.biogeosciences-discuss.net/8/7257/2011/
doi:10.5194/bgd-8-7257-2011

Biogeosciences Discussions

Modeling the vertical soil organic matter profile using $^{210}Pb_{ex}$ measurements and Bayesian inversion

M. C. Braakhekke[1,2,3], T. Wutzler[1], M. Reichstein[1], J. Kattge[1], C. Beer[1], M. Schrumpf[1], I. Schöning[1], M. R. Hoosbeek[2], B. Kruijt[2], and P. Kabat[2]

[1]Max Planck Institute for Biogeochemistry, P.O. Box 100164, 07701 Jena, Germany
[2]Wageningen University, Department of Environmental Sciences, Earth System Science and Climate Change Group, P.O. Box 47, 6700AA Wageningen, The Netherlands
[3]International Max Planck Research School on Earth System Modelling, Hamburg, Germany

Received: 9 May 2011 – Accepted: 4 July 2011 – Published: 21 July 2011

Correspondence to: M. C. Braakhekke (maarten.braakhekke@bgc-jena.mpg.de)

Published by Copernicus Publications on behalf of the European Geosciences Union.

Abstract

In view of its potential significance for soil organic matter (SOM) cycling, the vertical SOM distribution in the profile should be considered in models. To mechanistically predict the SOM profile, three additional processes should be represented compared to bulk SOM models: (vertically distributed) rhizodeposition, mixing due to bioturbation, and movement with the liquid phase as dissolved organic matter. However, the convolution of these processes complicates parameter estimation based on the vertical SOM distribution alone. Measurements of the atmospherically produced isotope $^{210}Pb_{ex}$ may provide the additional information needed to constrain the processes. Since $^{210}Pb_{ex}$ enters the soil at the surface and bind strongly to organic matter it is an effective tracer for SOM transport. In order to study the importance of root input, bioturbation, and liquid phase transport for SOM profile formation we performed Bayesian parameter estimation of the previously developed mechanistic SOM profile model SOMPROF. 13 parameters, related to decomposition and transport of organic matter, were estimated for the soils of two temperate forests with strongly contrasting SOM profiles: Loobos (the Netherlands) and Hainich (Germany). Measurements of organic carbon stocks and concentrations, decomposition rates, and $^{210}Pb_{ex}$ profiles were used in the optimization. For both sites, 3 optimizations were performed in which stepwise $^{210}Pb_{ex}$ data and prior knowledge were added. The optimizations yielded posterior distributions with several cases (modes) which were characterized by the dominant organic matter (OM) pool: non-leachable slow OM, leachable slow OM, or root litter. For Loobos, the addition of $^{210}Pb_{ex}$ data to the optimization clearly indicated which case was most likely. For Hainich, there is more uncertainty, but the most likely case produced by the optimization agrees well with other measurements. For both sites the most likely case of the final optimization was one where leachable slow OM dominates, suggesting that most organic matter is adsorbed to the mineral phase. Liquid phase transport (advection) of OM was responsible for virtually all organic matter transport for Loobos, while for Hainich bioturbation (diffusion) and liquid phase transport were of comparable

BGD

8, 7257–7312, 2011

magnitude. These results are in good agreement with the differences between the two sites in terms of soil texture and biological activity.

1 Introduction

To reduce the uncertainty of terrestrial carbon exchange predictions, it is crucial to improve understanding of soil carbon cycling, and to transfer this knowledge to numerical models (Heimann and Reichstein, 2008; Trumbore, 2009; Reichstein and Beer, 2008). Increasing evidence indicates that soil organic matter decomposition and stabilization is controlled by a range of mechanisms that depend on physical, chemical, and biological factors (von Lützow et al., 2006). While these factors vary laterally at landscape scale in relation to climate, vegetation and soil type, they change over centimeters to meters, within the vertical soil profile. Since most drivers (e.g. wetting, heating, organic matter input) are exerted on the soil at the surface, most soil properties have strong depth gradients. Consequently, the conditions that determine soil carbon cycling are highly depth-dependent and different mechanisms may be operating in different layers within one profile (Rumpel et al., 2002; Salomé et al., 2010; Rumpel and Kögel-Knabner, 2011). Therefore, aggregation of properties and processes over the profile, as is currently done in most SOM models (e.g. Parton et al., 1987; Schimel et al., 1994), is likely an oversimplification, inadequate to support new parameterizations of relevant processes.

Awareness of this problem has spurred recent efforts to develop models that predict the vertical distribution of SOM, based on explicit descriptions of carbon deposition processes in the profile (Jenkinson and Coleman, 2008; Koven et al., 2009; Braakhekke et al., 2011). In most soils there are three mechanisms by which organic carbon can be input at any given depth in the profile: (i) Organic matter may be deposited in situ by rhizodeposition: root exudation, sloughing off of root tissue and root turnover. (ii) Mobile (mainly dissolved and to a lesser degree colloidal) organic matter fractions may be transferred within the profile due to movement with the liquid phase. This type of

BGD
8, 7257–7312, 2011

transport is of advective nature, although the transport rate likely varies with depth in the profile, depending on average water fluxes and soil texture. (iii) Downward dispersal of organic matter occurs due to mixing of the soil matrix. Soil mixing is mostly caused by bioturbation (the reworking activity of soil animals and plant roots) and its effects on organic matter may be simulated mathematically as diffusion, provided the time and space scale of the model are sufficiently large (Boudreau, 1986; Braakhekke et al., 2011).

The processes involved in SOM deposition in the profile – rhizodeposition, liquid phase transport, and bioturbation – are fundamentally different, not only in a physical and mathematical sense, but also in terms of their relationship with environmental factors. Therefore, in order for a SOM profile model to be robust over different ecosystems and soil types, and over changing environmental conditions, the relevant processes should be explicitly represented, and their rates individually constrained. Unfortunately, the different processes have been poorly quantified to this date. Published results are inconsistent and past studies have generally focused on a single mechanism, rather than comparing all three (Rasse et al., 2005; Kaiser and Guggenberger, 2000; Tonneijck and Jongmans, 2008). The extremely low rates, as well as practical problems impede direct measurements of these processes in the field. Furthermore, the fact that the mechanisms are acting simultaneously complicates inference from SOM profile measurements. Diffusion and advection of decaying compounds such as organic matter, often produce very similar concentration profiles, despite the different natures of these processes. At the same time, root litter input closely follows the root biomass distribution, which often strongly resembles the SOM profile. Hence, it is generally not possible to derive the rate of each process from the organic carbon profile alone, unless strong assumptions are made. A model that includes all relevant processes can likely produce very similar SOM profiles with entirely different parameter combinations – a problem referred to as equifinality (Beven and Freer, 2001).

Thus, additional information is required in order to parameterize dynamic SOM profile models. In past studies, ^{13}C and ^{14}C, have been used as tracers to this purpose

BGD
8, 7257–7312, 2011

(Elzein and Balesdent, 1995; Freier et al., 2010; Baisden et al., 2002). Although these isotopes are particularly useful for constraining organic matter turnover times and carbon pathways, their precise information content with respect to the processes involved in SOM profile formation is less clear, since rhizodeposition leads to direct input of ^{13}C and ^{14}C at depth.

In this context, fallout radio-isotopes (e.g. ^{137}Cs, ^{134}Cs, $^{210}Pb_{ex}$, ^{7}Be) may be more effective. Such tracers have two major advantages over carbon isotopes: (i) loss occurs only due to radioactive decay, which is constant and exactly known; and (ii) input occurs only at the soil surface – direct input at depth is negligible. These points imply that the vertical transport rate of such isotopes can be directly inferred from their concentration profile (Kaste et al., 2007; He and Walling, 1997). Many radio-isotopes sorb strongly to organic matter molecules. Transport independent from the sorbent can be considered negligible for such isotopes, hence they offer an effective alternative or complement to carbon isotopes for inferring transport processes in soils (Dörr and Münnich, 1989, 1991). Particularly $^{210}Pb_{ex}$ (^{210}Pb in excess of the in situ produced fraction) is a valuable tracer due to its strong adsorption to soil particles, and relatively constant fallout rate (Walling and He, 1999). Past studies have mostly used radio-isotopes for determining erosion and deposition rates (Mabit et al., 2009; Wakiyama et al., 2010), while their use for inferring vertical transport at stable sites has received little attention (Dörr and Münnich, 1989; Kaste et al., 2007; Yoo et al., 2011).

The aim of this study was to examine SOM profile formation with model inversion. We used $^{210}Pb_{ex}$ concentration profiles, in addition to soil carbon measurements, to optimize the model SOMPROF for two forest sites with contrasting SOM profiles. SOMPROF (Braakhekke et al., 2011) is a vertically explicit SOM model that simulates the distribution of organic matter over the mineral soil profile and surface organic layers based on explicit descriptions of bioturbation, liquid phase transport, root litter input, and decomposition. We aimed to answer the following questions: (i) What is the relative importance of the different processes involved in SOM profile formation? (ii) How much organic matter is present as material potentially transportable with the liquid phase, as

BGD
8, 7257–7312, 2011

compared to immobile particulate material? And, (iii) what is the information content of $^{210}Pb_{ex}$ profile data and organic carbon measurements with respect to the optimized parameters? For both sites, 13 parameters, related to decomposition and transport of organic matter, were estimated. The model inversion was performed in a Bayesian framework, allowing us to include prior knowledge on the model parameters and to estimate their posterior uncertainty.

2 Methods

2.1 The SOMPROF model

Here a brief overview of SOMPROF is presented. We focus specifically on the model components related to the optimized parameters and the lead-210 module. A more exhaustive description and the rationale behind the model structure is presented in Braakhekke et al. (2011).

In SOMPROF the soil profile is explicitly split into the mineral soil and the surface organic layer, which is assumed to contain no mineral material and is further subdivided into three horizons: L, F and H (Fig. 1). These organic horizons are simulated as homogeneous connected reservoirs of organic matter (OM). Immobile decomposition products of litter flow from the L to the F horizon and from the F to the H horizon. Additionally, material may be transported downward between the organic horizons and into the mineral soil by bioturbation. For the mineral soil, which comprises both organic matter and mineral material, the model simulates the vertical distribution of each organic matter pool, using a diffusion-advection model.

The SOMPROF simulations in this study were started without any organic carbon in the profile. The model was run with a time step length of one month (1/12 yr), for a specified maximum number of years, and was driven by average annual cycles of soil temperature, moisture and (root) litter production.

BGD
8, 7257–7312, 2011

2.1.1 Organic matter pools and decomposition

The organic matter in the model comprises five organic matter pools representing organic matter types that differ with respect to decomposability, transport behavior and mechanism of input: above ground litter (AGL), fragmented litter (FL), root litter (RL), non-leachable slow organic matter (NLS), and leachable slow organic matter (LS). Above ground and root litter are externally input; fragmented litter and leachable and non-leachable slow OM are formed by decomposition. Note that the LS-OM pool represents *potentially* leachable material; the bulk of this organic matter is in fact immobile due to the adsorption to the mineral phase. LS-OM is absent in the organic horizons since the adsorptive capacity there is assumed to be negligible compared to that of the mineral soil.

Organic matter decomposition is simulated as a first-order decay flux, corrected for soil temperature and moisture. For any organic matter pool i decomposition is defined as:

$$L_i = f(T)\, g(W)\, k_i C_i\,, \tag{1}$$

where C_i is the concentration ($\mathrm{kg\,m^{-3}}$, for the mineral soil) or the stock ($\mathrm{kg\,m^{-2}}$, for the organic horizons), k_i is the decomposition rate ($\mathrm{yr^{-1}}$) at 10 °C and optimal soil moisture, and $f(T)$ and $g(W)$ are response functions for soil temperature and moisture (see Braakhekke et al., 2011).

The formation of fragmented litter, non-leachable and leachable slow OM is defined according to a transformation factor ($\alpha_{i\to j}$) which specifies how much of the decomposition flux of the donor pool i flows into the receiving pool j:

$$F_{i\to j} = \alpha_{i\to j} L_i\,. \tag{2}$$

The organic matter that does not flow to other pools is assumed to be lost as CO_2.

BGD
8, 7257–7312, 2011

2.1.2 Organic matter transport

All organic matter pools except above ground litter are transported by bioturbation, at the same rate. Conversely, only the leachable slow organic matter pool is transported by advection. All transport parameters are constant and independent of depth.

For the organic layer, organic matter transport due to bioturbation is determined by the bioturbation rate B ($\mathrm{kg\,m^{-2}\,yr^{-1}}$), which represents the mixing activity of the soil fauna, i.e. the amount of material being displaced per unit area and unit time. B is the maximum potential flux of organic matter that can be moved downward. In case the potential bioturbation flux cannot be met by the organic matter pools in a horizon, it is adjusted downward.

For the mineral soil, a diffusion model is applied to simulate transport due to bioturbation:

$$\left.\frac{\partial C_i}{\partial t}\right|_{\mathrm{BT}} = D_{\mathrm{BT}} \frac{\partial^2 C_i}{\partial z^2}, \tag{3}$$

where C_i is the local concentration of organic matter pool i ($\mathrm{kg\,m^{-3}}$), z is depth in the mineral soil (m, positive downward; $z = 0$ at the top of the mineral soil), and t is time (yr). (D_{BT} is the diffusivity ($\mathrm{m^2\,yr^{-1}}$) which is derived from the bioturbation rate according to mixing length theory, as follows:

$$D_{\mathrm{BT}} = \tfrac{1}{2} \frac{B}{\rho^{\mathrm{MS}}} l_{\mathrm{m}}, \tag{4}$$

where is ρ^{MS} is the local bulk density ($\mathrm{kg\,m^{-3}}$), and l_{m} is the mixing length (m), a tuning parameter that links the bioturbation rate to the diffusivity. The upper boundary condition, at the top of the mineral soil, is determined by flux of material coming from the H horizon, as determined by B.

Dissolved organic matter is not explicitly represented in SOMPROF. Instead, the combined effects of ad- and desorption and water flow on the concentration profile of

BGD
8, 7257–7312, 2011

the leachable organic matter pool are simulated as an effective advection process:

$$\left.\frac{\partial C_{\mathrm{LS}}}{\partial t}\right|_{\mathrm{adv}} = -v\frac{\partial C_{\mathrm{LS}}}{\partial z}, \tag{5}$$

where v is the effective organic matter advection rate ($\mathrm{m\,yr^{-1}}$). Note that the LS-OM pool is also transported by bioturbation. The upper boundary condition for this pool is determined by the total production in the organic layer. For the lower boundary, a zero-gradient boundary condition is used for all pools, hence only advection can lead to a loss of organic matter by transport.

2.1.3 $^{210}Pb_{ex}$ simulation

Lead-210 is a radiogenic isotope that is input into the soil both due to atmospheric deposition and in situ formation within the profile. The the fallout fraction ($^{210}Pb_{ex}$) is typically estimated as the difference between the total lead-210 activity and the activity of ^{226}Ra which is a precursor of ^{210}Pb (Appleby and Oldfield, 1978).

A module has been added to SOMPROF in order to use measurements of excess lead-210 as a tracer for SOM transport (Fig. 1). The modeled $^{210}Pb_{ex}$ concentration profile is controlled by atmospheric input, radioactive decay, and organic matter input, decomposition and transport. The $^{210}Pb_{ex}$ module is based on the following assumptions: (i) variations in time of the atmospheric $^{210}Pb_{ex}$ input are negligible; (ii) $^{210}Pb_{ex}$ is input only into the L horizon, where it is immediately bound to organic matter; the time needed for adsorption is negligible; (iii) $^{210}Pb_{ex}$ binds equally well to all organic matter fractions; (iv) no $^{210}Pb_{ex}$ is associated to root litter or its decomposition products; (v) the adsorption of $^{210}Pb_{ex}$ is irreversible, hence it is not transported independently of organic matter; (vi) ^{210}Pb "follows" the organic matter to which it is bound through the decomposition and transport processes; and (vii) aside from transport, $^{210}Pb_{ex}$ is lost only due to radioactive decay, at a fixed rate of $0.0311\,\mathrm{yr^{-1}}$.

BGD
8, 7257–7312, 2011

The transport behavior of $^{210}Pb_{ex}$ follows that of the organic matter pool to which it is associated. Furthermore, input of organic matter as above ground litter or root litter deposition has a diluting effect on $^{210}Pb_{ex}$, while loss of organic matter as CO_2 leads to an increase of concentration. For the organic horizons, the $^{210}Pb_{ex}$ fluxes due organic matter flow (either by transport or transformation to another pool) are calculated by multiplying the flux from a pool with its $^{210}Pb_{ex}$ mass fraction. For the mineral soil the transport equations are solved separately for $^{210}Pb_{ex}$ associated with fragmented litter, NLS-OM and LS-OM.

The atmospheric deposition rate of $^{210}Pb_{ex}$ is not generally known. However, since we are only interested in the relative change of concentration with depth – not the absolute concentrations – the input is set to 1 (see also Sect. 2.3.2).

2.2 Site descriptions

2.2.1 Loobos

Loobos is a Scots pine (*Pinus sylvestris*) forest on a well drained, sandy soil in the Netherlands (52°10′0″ N; 5°44′38″ E). The climate is temperate/oceanic with an average annual precipitation of 966 mm and an average temperature of 10 °C (WUR, Alterra, 2011). The area was originally covered by shifting sands but in the early twentieth century forest was planted. The forest floor is covered with a dense understorey of wavy hair grass (*Deschampsia flexuosa*) that roots primarily in the organic layer. Due to its young age, the soil is classified as Cambic or Haplic Arenosol (IUSS Working Group WRB, 2007; Smit, 1999), but it shows clear signs of podzolization. Due to the high content of quartzitic sand (> 94 %) the soils are pedologically very poor, reflected by a low pH (3–4) and nutrient concentration and a virtual absence of soil fauna (Emmer, 1995; Smit, 1999). As a result, most organic carbon is present in a thick organic layer of circa 11 cm, and organic carbon fractions in the mineral soil are very low.

BGD
8, 7257–7312, 2011

Half-hourly measurements of soil moisture and temperature are performed continuously at five depths (5, 13, 30, 60, 110 cm). Data for the period 1 May 2005 to 31 December 2008 was used to derive an average annual cycle of soil temperature and moisture which was used for the simulations. Additionally, above ground litter fall measurements for the period 2000 to 2008 on a two to four weeks basis were used to derive an average annual cycle for above ground litter input. Since the carbon content of the litter was not determined, we used a fixed C fraction of 50 %.

The grass understorey accounts for almost two thirds of the organic matter input, mostly by root turnover (Table 1). Annual root litter input was taken from Smit et al. (2001) who estimated root litter production using root ingrowth cores. To account for seasonal fluctuations of the grass layer, the annual input of both above and below ground grass litter production was distributed over the year using a function based on data taken from Veresoglou and Fitter (1984), which peaks around early June. The vertical distribution of root litter input was set such that approximately 95 % occurs in the organic layer (Supplement Fig. 1), which corresponds in situ observations of root biomass (A. Smit, personal communication, 2009).

The simulation length was set to 95 yr, which is approximately the time between the forest plantation and the sampling date. To account for the time needed for vegetation to develop, litter input is reduced in the initial stage, by multiplying with a function linearly increasing from 0, at the start of the simulation, to 1, after 60 yr (Emmer, 1995).

2.2.2 Hainich

This site is located in the Hainich national park in central Germany, (51°4′45.36″ N; 10°27′7.20″ E). The forest, which has been unmanaged for the last 60 yr, is dominated by beech (*Fagus Sylvatica*, 65 %) and ash (*Fraxinus excelsior*, 25 %) (Kutsch et al., 2010). The forest floor is covered by herbaceous vegetation (*Allium ursinum*, *Mercurialis perennis*, *Anemone nemorosa*) which peaks before canopy budbreak. The climate is temperate suboceanic/subcontinental with an average annual precipitation of 800 mm and an average temperature of 7 to 8 °C.

BGD
8, 7257–7312, 2011

The soil is classified as Luvisol or Cambisol (IUSS Working Group WRB, 2007; Kutsch et al., 2010). It has formed in limestone overlain by a layer of loess, and is characterized by a high clay content (60 %) and a pH-H_2O of 5.9 to 7.8 (T. Persson, personal communication, 2011). The favorable soil properties support a high biological activity (Cesarz et al., 2007), corroborated by a thin organic layer and a well developed A horizon. About 90 % of the root biomass occurs above 40 cm depth (Supplement Fig. 1).

The Hainich simulation has been set up identically to that presented in Braakhekke et al. (2011) (reference simulation). For additional information we refer to this publication. The not-optimized model input is listed in Table 1.

2.3 Observations used for optimization

2.3.1 Carbon measurements

For Loobos, measured carbon stocks in the L, F and H horizon and the mineral soil, and carbon mass fractions at 3 depths in the mineral profile were used in the optimization. Several profiles were affected by wind erosion. When this was the case, the affected measurements were omitted.

In 2005 the soil was sampled in a regular quadratic grid at 25 points spaced 40 m apart. Organic layers were removed with a square metal frame with a side length of 25 cm. The mineral soil was sampled horizon-wise with a Pürckhauer auger, 2–3 cm wide and 1 m long. Bulk density of the upper 5 cm of the mineral soil was determined with three 100 cm^3 cylinders at each of the 25 grid points. In view of low spatial variability, the bulk densities of the subsoil horizons were derived from a representative soil pit in the center of the study area. Soil samples were sieved to < 2 mm and ground. Carbon stocks in the organic layers were analyzed with a CN analyser Vario EL (Elementar Analysensysteme GmbH, Hanau, Germany); carbon fractions in the mineral soil were measured with a CN Analyser VarioMax (Elementar Analysensysteme GmbH, Hanau, Germany).

BGD
8, 7257–7312, 2011

For Hainich, measured stocks in the L and F/H horizon (the individual F and H horizons could not be identified), and in the mineral soil were used, as well as mass fraction measurements at 8 depths in the mineral profile. In addition, we used measured effective decomposition rates at 15 °C and optimal soil moisture in the L and F/H horizon, and at 7 depths in the mineral profile. The sampling procedure and organic carbon measurements are described in Schrumpf et al. (2011). The decomposition rates were calculated from measurements of respiration rates measured during lab incubation of soil samples which are described in Kutsch et al. (2010). By dividing the average respiration rate of each sample by its organic carbon content, we obtained effective decomposition rates.

2.3.2 $^{210}Pb_{ex}$ measurements

Since local $^{210}Pb_{ex}$ measurements were not available for Loobos, we used two activity profiles from Kaste et al. (2007), for a site in the Hubbard Brook Experimental Forest, New Hampshire, USA. This site has conditions similar to those at Loobos in terms of vegetation, soil texture, soil pH, and soil biological activity (Bormann and Likens, 1994). Furthermore, pedological processes related to podzol formation are occurring at both sites. The two sites differ with respect to age, since the Loobos soil is very young. However, in view of the relatively fast decay rate of ^{210}Pb, and the shallowness of the $^{210}Pb_{ex}$ profile (Fig. 2), we assume that it is close to steady state at both sites.

For Hainich, local $^{210}Pb_{ex}$ measurements were taken from Fujiyoshi and Sawamura (2004). Although these measurements were corrected for in situ formed ^{210}Pb by subtracting ^{226}Ra activity (R. Fujiyoshi, personal communication, 2008), the activity profile did not approach zero with depth, hence this method did presumably not account for all supported ^{210}Pb. Therefore, we assumed that the supported $^{210}Pb_{ex}$ concentration is zero from approximately 12.5 cm downwards. The the supported ^{210}Pb activity was estimated as the average below this depth, and all data was corrected by subtracting this average. (Note that in several cases this produced negative concentrations.)

BGD
8, 7257–7312, 2011

The activity data from both sites were normalized using the $^{210}Pb_{ex}$ activity at the surface of the mineral soil which was estimated using piecewise Hermitian extrapolation. Since neither data set had sufficient replicate measurements to estimate spatial variability, a one-parameter exponential model was fit to the normalized depth distribution, and the uncertainty used for the optimization was estimated as the standard error of the prediction. The thus obtained profiles and standard errors are shown in Fig. 2.

2.4 Bayesian optimization

We performed Bayesian estimation of 13 model parameters: 5 decomposition rates, 5 transformation factors, and 3 transport parameters (Table 2). Bayesian parameter estimation is aimed at deriving the posterior probability distribution $P(\boldsymbol{\theta}|\boldsymbol{O})$ of the model parameters $\boldsymbol{\theta}$ based on the misfit between the model results and the observations $\boldsymbol{O}$, and the a priori probability distribution of the parameters $P(\boldsymbol{\theta})$ (Mosegaard and Sambridge, 2002). Here, $\boldsymbol{\theta}$ is a vector containing all model parameters that are optimized. According to Bayes' theorem, the posterior distribution is defined as:

$$P(\boldsymbol{\theta}|\boldsymbol{O}) = c\,P(\boldsymbol{\theta})\,L(\boldsymbol{O}|\boldsymbol{\theta}), \quad (6)$$

where $P(\boldsymbol{\theta})$ is the prior probability distribution, expressing our knowledge of the parameters prior to the optimization. The normalization constant c assures that $\int_{-\infty}^{\infty} P(\boldsymbol{\theta}|\boldsymbol{O})\mathrm{d}\boldsymbol{\theta} = 1$, which is a requirement of a proper probability density function. $L(\boldsymbol{O}|\boldsymbol{\theta})$ is a likelihood function that expresses the probability of measuring $\boldsymbol{O}$, given the parameters $\boldsymbol{\theta}$ (Gelman et al., 1995, ch. 1). Hence, $L(\boldsymbol{O}|\boldsymbol{\theta})$ essentially maps the probability distribution of the measurements to the parameter space $\boldsymbol{\theta}$, based on the inverted model structure.

Due to the complexity of the model, no analytical expression of the posterior distribution exists for our case. We therefore used a Markov Chain Monte Carlo (MCMC) approach which obtains a random sample of $P(\boldsymbol{\theta}|\boldsymbol{O})$ by performing a random guided walk in parameter space. The posterior sample is comprised of all the steps of the

BGD
8, 7257–7312, 2011

random walk. MCMC algorithms are increasingly used due to the rising availability of computational resources as well as the increasing amount of data becoming available from e.g. eddy-covariance flux measurements and satellite observations (Fox et al., 2009). They have also been applied to optimize soil carbon models (Yeluripati et al., 2009; Scharnagl et al., 2010; de Bruijn and Butterbach-Bahl, 2010). We used the well-known Metropolis-Hastings algorithm which is further described in Appendix A1.

2.4.1 Uncertainty of the observations

In order to obtain the likelihood function $L(\boldsymbol{O}|\boldsymbol{\theta})$, an uncertainty model for the measured variables must be defined. Since all observed quantities are bounded at zero, we assumed a log-normal distribution. The total likelihood of the model results was determined by combining the misfit of all the different types of observed quantities (e.g. the organic carbon fraction at a certain depth, the stock in the L horizon, etc.):

$$L(\boldsymbol{O}|\boldsymbol{\theta}) = \exp\left(-\frac{1}{2}\sum_{i=1}^{I} C_i(\boldsymbol{\theta},\boldsymbol{O})\right), \quad (7)$$

where I is the number of different types of observations and $C_i(\boldsymbol{\theta},\boldsymbol{O})$ is the cost, which expresses the misfit of the model results to measurement type i. Note that we did not consider correlations between the measurements.

For any type of measurement i, the cost was determined from the individual replicates of each type of observation:

$$C_i(\boldsymbol{\theta},\boldsymbol{O}) = \sum_{j=1}^{J_i}\left(\frac{\ln(M_i(\boldsymbol{\theta})) - \ln(O_{i,j})}{\sigma_{\ln(O_i)}}\right)^2, \quad (8)$$

where J_i is the number of replicates, $M_i(\boldsymbol{\theta})$ is the model prediction, $O_{i,j}$ is the value of replicate measurement j, and $\sigma_{\ln(O_i)}$ is the sample standard deviation over all log-transformed replicates.

BGD
8, 7257–7312, 2011

2.4.2 Prior parameter distributions

We performed MCMC runs with both strong and with weak prior distributions. For the weak priors, the prior probability $P(\boldsymbol{\theta})$ was simply omitted from the posterior distribution, which resulted in a multivariate uniform distribution, within the sampling region.

For the runs with strong priors, the distributions were based on knowledge obtained from previously published studies (Braakhekke et al., 2011). The same distributions were used for both sites. The priors of the decomposition rates were log-normal, since these parameters have their theoretical minimum at 0. For the litter pools (k_{AGL}, k_{RL} and k_{FL}) we used the same distributions, with a maximum likelihood at 0.20 yr^{-1} (Fig. 3a). It is likely that the decomposition rate of leachable slow organic matter (k_{LS}) is lower than that of non-leachable slow organic matter (k_{NLS}), since the former is comprised mostly of material adsorbed to the mineral phase. Nevertheless, since we aimed to test this hypothesis with the measurements, we used the same prior distributions for the decomposition rate of both pools (maximum likelihood at 0.014 yr^{-1}; Fig. 3b).

We used logit-normal prior distributions for the transformation factors. This distribution is similar to the beta distribution and is bounded between 0 and 1 (Mead, 1965). For $\alpha_{\mathrm{AGL}\rightarrow\mathrm{FL}}$ a distribution with maximum likelihood at 0.83 was used (Fig. 3c), while for the other conversion fractions ($\alpha_{\mathrm{RL}\rightarrow\mathrm{NLS}}$, $\alpha_{\mathrm{RL}\rightarrow\mathrm{LS}}$, $\alpha_{\mathrm{FL}\rightarrow\mathrm{NLS}}$, and $\alpha_{\mathrm{FL}\rightarrow\mathrm{LS}}$) the same prior was used with the maximum likelihood at 0.057 (Fig. 3d). Since relatively little a priori information about the SOM transport parameters (B, l_m, and v) is available, we used uniform priors within the sampling region for all optimizations (Fig. 3e).

The optimization was constrained to a bounded region in parameter space (Table 2) since preliminary runs showed that, in certain cases, several parameters were virtually unconstrained at the upper bound by the data. Furthermore, since decomposition cannot lead to a net formation of material, the sum of transformation factors for root litter ($\alpha_{\mathrm{RL}\rightarrow\mathrm{NLS}} + \alpha_{\mathrm{RL}\rightarrow\mathrm{LS}}$) and fragmented litter ($\alpha_{\mathrm{FL}\rightarrow\mathrm{NLS}} + \alpha_{\mathrm{FL}\rightarrow\mathrm{LS}}$) pools was bounded to 1.

BGD
8, 7257–7312, 2011

2.4.3 MCMC run setup and forward simulations

Three series of MCMC runs (referred to as optimization setups from hereon) were performed in which $^{210}Pb_{ex}$ data and prior knowledge were stepwise added, in order to investigate the information content of each source of information. Thus, for both sites, we ran optimizations in the following setups:

1. excluding $^{210}Pb_{ex}$ data and with weak priors;
2. including $^{210}Pb_{ex}$ data and with weak priors;
3. including $^{210}Pb_{ex}$ data and with strong priors.

Optimization setup 3 represents our best estimate of the model parameters.

To illustrate the results of the optimizations we performed forward Monte Carlo simulations based on the posterior distributions. 1000 simulations were made with parameter sets drawn randomly from the posterior samples. The setup of these simulations was the same as those made for the MCMC runs.

3 Results

For most of the optimization setups, the posterior distribution is multi-modal, meaning it has more than one local optimum. For most optimizations the posterior modes are very distant and isolated in parameter space. Hence they represent distinctly different explanations for the measurements, in terms of the processes that are included in the model. We refer to the modes as "cases" in the discussions below.

When a clear favorite case can be identified for a given optimization setup, the other cases often have negligible probability. Nevertheless, we also report several non-favorite cases here because they are illustrative of the workings of the model and demonstrate the usefulness of the Bayesian approach in combination with $^{210}Pb_{ex}$ data. We show the distributions separately for all cases of interest and report the

BGD
8, 7257–7312, 2011

value of the lowest total cost (summed over all measurements, cf. Eq. 8) in the sample for each case, as an indicator of its performance[1]. It must be noted that for different cases within the same optimization setup, the *absolute* difference between the costs determines the difference in probability, not the relative difference.

The continuous posterior distributions depicted in the figures were derived using kernel density estimation.

3.1 Loobos

3.1.1 Setup 1: excluding $^{210}Pb_{ex}$ data; weak priors

The posterior distribution for the setup 1 (excluding $^{210}Pb_{ex}$ and with weak priors) for Loobos has two cases with distinctly differing marginal distributions for several parameters (Fig. 4a). The value of the minimum cost (Table 3) indicates that case B performs significantly better at fitting the measurements.

The contrast between the two cases is further demonstrated by the results of the forward simulations (Fig. 5). While non-leachable slow (NLS) organic matter is the largest pool in case A, the leachable slow (LS) OM pool dominates in case B. These differences can be attributed mostly to the decomposition rates of these pools. The difference in average performance is also apparent from Fig. 5: case B performs significantly better at reproducing the organic matter stocks and profile.

3.1.2 Setup 2: including $^{210}Pb_{ex}$ data; weak priors

Adding $^{210}Pb_{ex}$ measurements to the observations used in the optimization has a large effect on the posterior (Fig. 4b). Again, two cases exist in which either NLS-OM or LS-OM is the dominant organic matter pool (Supplement Fig. 3). However, particularly

[1]Note that the lowest cost in the sample is likely an overestimation of the cost at the true minimum. This is because the algorithm does not necessarily come close to the true minimum, due to the high number of dimensions.

BGD
8, 7257–7312, 2011

for case A, the marginal distributions of several parameters differ strongly with respect to optimization 1.

Compared to the optimization without $^{210}Pb_{ex}$, the average cost of case A has increased dramatically while the cost of case B has increased only slightly (Table 3; Supplement Fig. 2). The reason for the different performance of the two cases is clear from the $^{210}Pb_{ex}$ results of the forward runs (Fig. 6): for case A the model completely fails to reproduce the $^{210}Pb_{ex}$ profile, compared to case B. Also the fit to the organic carbon measurements has decreased for case A (Supplement Fig. 3).

3.1.3 Setup 3: including $^{210}Pb_{ex}$ data; strong priors

In the setup with $^{210}Pb_{ex}$ data and strong priors, only one case was found (Fig. 4c), in which LS-OM dominates. A case may still exist in which NLS-OM dominates, but the cost has presumably further increased due to the prior distributions. Compared to case B in the optimization setup 2, the distributions of several parameters (k_{NLS}, $\alpha_{FL\rightarrow NLS}$, $\alpha_{RL\rightarrow NLS}$ have changed to fit the prior distributions. Although uniform priors were used for the transport parameters, the bioturbation rate B, and mixing length l_m are well constrained. Contrastingly, the advection rate v is quite poorly constrained and apparently can be chosen freely from high end of the sampling range.

Despite the change of several of the marginal distributions, the results of the forward simulations are very similar to those of case B for setups 1 and 2 (Fig. 7). Figure 8 depicts the modeled vertical transport fluxes of the forward simulations. Virtually all organic matter movement occurs with as liquid phase transport.

3.2 Hainich

3.2.1 Setup 1: Excluding $^{210}Pb_{ex}$ data; weak priors

The optimization in setup 1 for Hainich produced 3 distinct cases in the posterior distribution (Fig. 9a). Case C has the lowest minimum cost (Table 3).

BGD
8, 7257–7312, 2011

Again there is a distinct contrast between the cases in terms of the contributions of each of the organic matter pools as demonstrated by the results of the forward simulations (Fig. 10). As for the optimizations for Loobos, there is a case in which NLS-OM dominates (A) and a case where LS-OM dominates (B). In addition, there is a case where root litter dominates (C). The better performance of case C is explained by the better fit of the model output to the the measured effective decomposition rate in the deep soil.

3.2.2 Setup 2: including $^{210}Pb_{ex}$; weak priors

When $^{210}Pb_{ex}$ was included in the optimization again three cases were found, with similar quantities of each organic matter pool, compared to the cases of setup 1 (Supplement Fig. 6). The addition of $^{210}Pb_{ex}$ data to the observations did not lead not significant changes in the marginal posterior distributions (Fig. 9b), with the exception of k_{LS} in case A.

The misfit to the $^{210}Pb_{ex}$ data has lead to an increase of the minimum cost for all cases (Table 3; Supplement Fig. 5), but more strongly so for case C, which is now higher than the other two cases. These results are illustrated by Fig. 11 which shows that $^{210}Pb_{ex}$ profile is better reproduced for cases A and B. (Other results are shown in Supplement Fig. 6.)

3.2.3 Setup 3: including $^{210}Pb_{ex}$; strong priors

In the optimization with $^{210}Pb_{ex}$ and strong priors, the three cases were again found by the algorithm. The minimum cost of case C has further increased (Table 3), to the point that we can discard it as explanation for the measurements. While cases A and B performed almost equally well in setup 2, the addition of prior information has shifted favor towards case B. Hence, we treat this case B as the most likely outcome of the optimization and show only results for this case. (The posterior distribution and results from forward simulations of case A and are shown in Supplement Figs. 7–10.)

BGD
8, 7257–7312, 2011

Compared to the prior distributions, significant constraint has been gained for most parameters, with the exception of k_{RL} (Fig. 9c). Figure 12 shows the results of the forward Monte Carlo runs for case B, which are very similar to those for setups 1 and 2. Figure 13 shows the modeled vertical transport rates for case B. In contrast to Loobos, bioturbation and liquid phase transport are of comparable magnitude in most of the profile.

3.3 Parameter correlations

Figure 14 depicts the correlations between the parameters for the most likely cases of optimization 3 (including $^{210}Pb_{ex}$ and with strong priors) for both sites. For both sites several strong correlations exist, which can mostly be explained well in the context of the model structure. For example, generally positive correlations exist between the parameters that control the formation of a specific organic matter pool (the transformation factor(s) $\alpha_{i \rightarrow j}$), and its decomposition rate, since these parameters combined control the total quantity of that pool. Also, the transport parameters are generally correlated with the parameters that are influenced by the respective transport processes. For both sites, the above ground litter decomposition rate k_{AGL} has little correlation with other parameters since this parameter is determined mostly by the measured carbon stock in the L horizon and, for Hainich, the effective decomposition rate in the L horizon. In the model, these quantities are fully determined by k_{AGL}.

4 Discussion

4.1 Loobos

For Loobos, the posterior distributions of all optimization setups have one clearly favorite case, allowing the most likely explanation for the observed vertical SOM profile to be identified. The results of the forward simulations for the final optimization suggest that the leachable slow (LS) pool is dominant type of organic matter (Fig. 7) and

BGD
8, 7257–7312, 2011

that liquid phase transport is responsible for virtually all organic matter movement in the mineral soil (Fig. 8). The relative importance of organic matter leaching is in good agreement with the soil characteristics at Loobos. Soil fauna is virtually absent, and the high concentration of sand supports fast water infiltration and has a low adsorptive capacity, thus allowing high dissolved organic matter (DOM) fluxes. Furthermore, the low soil pH may also further stimulate DOM fluxes since pH has been shown to be negatively correlated with DOM concentration (Michalzik et al., 2001).

Although SOMPROF was not developed to simulate DOM transport, the modeled liquid phase transport fluxes should represent the average movement of dissolved organic carbon (DOC) over long timescales[2]. Figure 8 shows that simulated liquid phase transport fluxes compare well to local measurements of DOC fluxes performed by Kindler et al. (2011), but are overestimated in the topsoil. However, the uncertainty of the simulated fluxes is quite high, indicating that the observations used in the optimization could also be explained with somewhat lower transport rates. Furthermore, the fit of the modeled liquid phase transport flux for case A of optimization 2 is markedly worse (Supplement Fig. 4).

The root litter input distribution for Loobos was set such that almost no input occurs below 5 cm in the mineral soil (Supplement Fig. 1) which explains why no case was found in which root litter dominates, as for the Hainich optimizations. This shallow distribution was chosen because the grass understorey, which is by far the largest source of root litter, roots primarily in the organic layer (A. Smit, personal communication, 2009). However, a small amount of root litter input from the pine canopy may still occur in the subsoil. Future study should explore the possible effects of this deep soil input on the results of the optimization.

It must be noted that due to the absence of in situ $^{210}Pb_{ex}$ measurements at Loobos, data from a different but similar site was used as a proxy. Comparison of the results

[2]Although the LS-OM represents mostly material adsorbed to the mineral phase, the transport of this pool occurs only by the small fraction that is mobile and thus corresponds to DOC fluxes.

BGD
8, 7257–7312, 2011

of optimizations setups 1 and 2 shows that adding $^{210}Pb_{ex}$ did not have a large effect on the forward results and the minimum cost for case B. This shows that the organic carbon and $^{210}Pb_{ex}$ profiles can be explained well together, suggesting that the $^{210}Pb_{ex}$ profile used for the optimization is consistent with that at Loobos.

4.2 Hainich

Despite the larger amount of data that is available for Hainich compared to Loobos, there is more uncertainty with respect to the three cases that were found. Case C, in which root litter dominates, can be discarded as unlikely with some confidence, in view of the its high cost compared to the other cases, in optimization setup 3.

Although the difference in minimum cost between case A and B (in which NLS-OM and LS-OM dominate) is considerably smaller, case B is still several orders magnitude more probable than case A in a purely statistical sense (cf. Eq. 7). However, in addition to the spread of the measurements, there are several uncertainties related to the assumption of steady state, possible effects of past land use and climate. Since these uncertainties were not represented in the optimization (see Sect. 4.5), the results as such are not sufficient to fully dismiss case A.

Organic matter density fractionation measurements (M. Schrumpf, unpublished data, 2011) indicate that 81–93 % of the organic matter is present in the heavy fraction, which is known to comprise mostly material in organo-mineral complexes (Golchin et al., 1994). Although the model pools can presumably not be compared directly to the measured density fractions, this is clearly in support of case B, since leachable slow OM represents mostly material adsorbed to the mineral phase (Sect. 2.1.2; Braakhekke et al., 2011).

Further confidence in case B is gained when comparing the modeled liquid phase transport fluxes with in situ measurements of DOC fluxes of Kindler et al. (2011). As depicted in Fig. 13, the modeled liquid phase transport fluxes for case B compare well to measured DOC fluxes, while the fit for case A and C (Supplement Fig. 10) is

BGD
8, 7257–7312, 2011

considerably worse. Despite the high concentration of leachable slow OM in case B, the liquid phase fluxes do not dominate, as for Loobos, which can be ascribed to the low advection rate.

4.3 Comparison between sites

The fact that for Hainich more data was used than for Loobos did not lead to significantly narrower marginal distributions. (Supplement Fig. 11). However, it is apparent from correlation structure (Sect. 4.4).

The fact that the above ground litter decomposition rate for Hainich is significantly lower than for Loobos is somewhat surprising since both sites have similar above ground litter input (Table 1), but Loobos has a significantly higher L horizon C stock ($1038 \pm 129\,\mathrm{gC\,m^{-2}}$ vs. $758 \pm 133\,\mathrm{gC\,m^{-2}}$ for Hainich). The discrepancy is caused by the fact that the measured moisture content in the L horizon for Loobos is quite low during summer, hence the model requires a high base decomposition rate to reproduce the observed stock. The moisture sensitivity of decomposition may be overestimated for Loobos.

The two sites differ strongly with respect to the organic matter transport parameters, with Hainich having higher values for the two parameters related to bioturbation, and Loobos having a much higher advection rate. This in good agreement with the differences between the two sites in terms of biological activity and soil texture.

Although at both sites leachable slow organic matter is the dominant pool, the decomposition rate of LS-OM is significantly lower for Hainich than for Loobos. Presumably, the effective decomposition rate measurements for the mineral soil for Hainich provide strong constraint for k_{LS}. Since for Loobos such information is not present, k_{LS} is only constrained by mineral soil organic matter fractions. Here, a decrease of k_{LS}, causing a lower loss of LS-OM by decomposition, can be compensated by an increase of v, causing a higher loss of LS-OM by advection, or by a decrease of $\alpha_{\mathrm{FL}\to\mathrm{LS}}$ and $\alpha_{\mathrm{RL}\to\mathrm{LS}}$, leading to lower production of this pool (cf. Fig. 14).

BGD
8, 7257–7312, 2011

4.4 Correlation structure and parameter identifiability

As shown in Fig. 14, there are many strong correlations between different combinations of model parameters, which indicates that the model is over-parameterized with respect to the available data. The correlations are generally less strong for Hainich than for Loobos which presumably is caused by the fact that for Hainich more data was used in the optimization. A consequence of the strong correlations is that the constraint of the posterior distributions is much stronger than what is suggested by the marginal distributions. The correlations between the parameters must be considered in order to determine the information gain of the observations (see also Supplement Fig. 12).

For all of the cases in all optimization setups there is at least one decomposition rate for which high values are not constrained by the observations (k_{RL} and k_{FL} for Loobos, Fig. 4c; and k_{FL} and k_{NLS} for Hainich, case B, Fig. 9c). Since the predicted stock of a pool is inversely proportional to its decomposition rate, this shows that SOMPROF has at least one redundant organic matter pool, given the available data. This is further demonstrated by the existence of several strong negative correlations between decomposition rates (k_{FL} and k_{RL} for Loobos and k_{FL} and k_{NLS} for Hainich), which suggest that organic matter pools are essentially "competing" as explanation for the observed carbon stocks and fractions. Further study should explore whether simplification of the model by removal of organic matter pools is warranted. If so, a possible solution would be to merge the root litter and fragmented litter pools, which are functionally very similar.

4.5 Methodological constraints and implications for soil organic matter cycling

In addition to the spread of the measurements there are several sources of uncertainty that were not, and in some cases *can* not, be considered in the Bayesian inversion. Examples include the behavior of $^{210}Pb_{ex}$ (discussed below), the general validity of the model structure, and the uncertainties discussed in Sects. 4.1 and 4.2. These uncertainties call for some care when interpreting the results in terms of the in situ

BGD
8, 7257–7312, 2011

processes. Furthermore, the case with the highest relative likelihood, should not be accepted offhand as the truth without verification.

Assuming that for both sites the most likely posterior case of optimization 3 is correct, our results emphasize the importance of organo-mineral interactions for soil carbon cycling. However, this conclusion relies on the assumption that mineral-associated organic matter is correctly represented by the LS-OM pool. Mathematically, the only difference between the NLS-OM and LS-OM pools in the model structure lies in the transport behavior. The question is whether this distinction correctly represents the differences between stable particulate and adsorbed organic matter in reality. The good agreement of our results with DOC flux and density fractionation measurements, as well as the environmental conditions at both sites suggests that a situation where LS-OM dominates might indeed be close to the truth. Furthermore, many studies have indicated the importance of mineral associations for long-term carbon preservation (Eusterhues et al., 2003; Mikutta et al., 2006; Kögel-Knabner et al., 2008; Kalbitz and Kaiser, 2008). In contrast, several researchers have indicated the presence of root-derived particulate material in podzol B horizons, and questioned the relevance of DOM transport for mineral soil organic matter fractions (Nierop, 1998; Nierop and Buurman, 1999; Buurman and Jongmans, 2005).

Our results also suggest that vertical transport of organic matter is the dominant process for the formation of the SOM profile at our sites. This contradicts Jobbagy and Jackson (2000), who proposed that root/shoot allocation together with the root biomass distribution controls the vertical SOM profile, based on analysis of a large database of SOM profiles. Also others have indicated the importance of root input for soil carbon (Rasse et al., 2005). However, our findings do not suggest that rhizodeposition is negligible for long term organic input compared to above ground litter production. The transformation factors indicate that the relative conversion to LS-OM is slightly higher for root litter than for fragmented litter. Furthermore, the contribution of root litter as a source of SOM will increase with depth in the profile. It is difficult to judge the source of SOM in the slow pools, since the material coming from fragmented litter and root litter

BGD
8, 7257–7312, 2011

are lumped in the model. In the future, the model will be modified to allow the source of of SOM to be traced.

4.6 The use of $^{210}Pb_{ex}$ measurements

For Loobos, the addition of $^{210}Pb_{ex}$ data was very helpful for disentangling the different processes involved in SOM profile formation. This is demonstrated by the vastly higher cost minimum for case B in optimization 2 compared to optimization 1. In contrast, the $^{210}Pb_{ex}$ data was much less informative for Hainich. Although the addition of $^{210}Pb_{ex}$ data reduced the likelihood of case C, in which root litter dominates, it did not help to disentangle the two transport mechanisms, as indicated by the similar costs minimum of case A and B, in optimization setup 2.

The difference between the two sites with respect to the information content of the $^{210}Pb_{ex}$ data may be partially explained by the less "ideal" shape of the $^{210}Pb_{ex}$ profile for Hainich, in the sense that it deviates from an exponentially decaying profile. Furthermore, the correction for supported ^{210}Pb activity (Sect. 2.3.2) created several negative values, which are intrinsically impossible to reproduce by the model.

The use of $^{210}Pb_{ex}$ as a tracer for SOM transport relies on the assumption that Pb adsorbs strongly to organic matter, both particulate and in solution. Based on $^{210}Pb_{ex}$ and ^{14}C profiles, Dörr and Münnich (1989) found that transport rates of $^{210}Pb_{ex}$ were very close to those of organic matter, suggesting that the two are indeed strongly linked. Although Pb is known to occur also in association with the mineral phase and inorganic complexes (Schroth et al., 2008), the affinity of Pb to particulate organic matter is well established, in view of its strong retention in organic layers and topsoils over short timescales (Kaste et al., 2003; Kylander et al., 2008; Schroth et al., 2008), as well as by adsorption studies (Logan et al., 1997; Sauve et al., 2000). The effect of DOM movement on Pb migration is less clear, because it is difficult to predict the behavior of Pb adsorbed to the organic matter that is transformed to the dissolved fraction. Several researchers have indicated the importance of DOM and colloidal organic carbon for Pb

BGD
8, 7257–7312, 2011

movement in soil (Miller and Friedland, 1994; Wang and Benoit, 1997; Urban et al., 1990; Friedland et al., 1992). Furthermore, adsorption studies have found that Pb adsorbs readily to humic and fulvic acids (Logan et al., 1997; Turner et al., 1986), while movement of dissolved Pb^{2+} was found to be insignificant (Wang and Benoit, 1997). In view of these past findings we believe that our use of $^{210}Pb_{ex}$ data to optimize SOMPROF is well defendable. However, further study focussing specifically on the use of $^{210}Pb_{ex}$ as a tracer for SOM transport, is needed.

5 Concluding remarks

We performed a Bayesian parameter estimation for 13 parameters of the SOMPROF model for two forest sites with strongly contrasting SOM profiles: Hainich and Loobos. The problem of equifinality caused by multiple processes acting simultaneously on the SOM profile (rhizodeposition, liquid phase transport, and bioturbation) is clearly illustrated by the existence of multiple modes (cases) in the posterior distribution, corresponding to distinctly different explanations for the observations. One clearly favorite case could be identified for Loobos. For Hainich there is more uncertainty, although the most likely case suggested by the optimization agrees well with other measurements.

In the most likely cases for both Loobos and Hainich, the leachable slow organic matter pool (representing material that can be moved with the liquid phase but is mostly adsorbed to minerals) has the lowest decomposition rate and thus comprises the bulk of the organic matter. The results indicate that two sites are characterized by different regimes in terms of organic matter transport. For Loobos, virtually all organic matter transport occurs by liquid phase transport, while for Hainich liquid phase transport and bioturbation fluxes are of comparable magnitude. These results agree well with local conditions at the sites.

Our study showed that organic carbon fractions and stocks are necessary but in general not sufficient for parameterizing a SOM profile model. $^{210}Pb_{ex}$ data represents a powerful tool that can offer much additional constraint on the model parameters, but

BGD
8, 7257–7312, 2011

not in all situations, as shown for Hainich. Other data may be considered to obtain additional constraint, such as other isotopes (^{14}C, ^{13}C, ^{15}N) and density fractionation measurements.

Future work will focus on deriving additional parameter sets for different soils and ecosystems to allow large scale simulations with SOMPROF. Bayesian optimization is an effective tool in this context since it allows knowledge obtained by previous optimizations to be re-used to construct new prior distributions.

Appendix A

Markov chain Monte Carlo scheme

A1 The Metropolis-Hastings algorithm

The Metropolis-Hastings algorithm (Metropolis et al., 1953; Hastings, 1970) samples the posterior distribution by performing a random guided walk in parameter space. At each iteration i a proposal sample of the parameters $\boldsymbol{\theta}^*$ is generated by taking a random step from the current sample $\boldsymbol{\theta}^i$. The model is run with the proposed parameter set and the unnormalized posterior likelihood ($P(\boldsymbol{\theta})L(\boldsymbol{O}|\boldsymbol{\theta})$) of the proposal is evaluated. The proposal is subsequently accepted or rejected according to the Metropolis-Hastings rule, which defines the chance for acceptance as:

$$s = \min\left\{\frac{L(\boldsymbol{O}|\boldsymbol{\theta}^*)P(\boldsymbol{\theta}^*)J(\boldsymbol{\theta}^i)}{L(\boldsymbol{O}|\boldsymbol{\theta}^i)P(\boldsymbol{\theta}^i)J(\boldsymbol{\theta}^*)}, 1\right\}, \tag{A1}$$

where $J(\boldsymbol{\theta})$ is the Hastings factor which may be included to remove the effects of an asymmetric proposal distribution (see Sect. A2). The decision for acceptance or rejection is made according to:

$$\theta^{i+1} = \begin{cases} \theta^* & \text{if } \alpha \leq s \\ \theta^i & \text{if } \alpha > s \end{cases}, \tag{A2}$$

BGD
8, 7257–7312, 2011

with $\alpha \sim \mathcal{U}(0,1)$.

We split the algorithm into three steps applied in cascade. The proposal sample is accepted or rejected based on: (i) the upper parameter bounds (see Table 2), (ii) the prior ($P(\boldsymbol{\theta})$) and, if applicable, the correction factor ($J(\boldsymbol{\theta})$), and (iii) the likelihood function ($L(\boldsymbol{O}|\boldsymbol{\theta})$). The algorithm proceeds only if the proposal is accepted in the current step, otherwise the sample is rejected for the complete iteration. This setup converges on the correct distribution, while reducing computation time since the model is only run if the proposal is accepted in the first step and second steps (Mosegaard and Tarantola, 1995; Knorr and Kattge, 2005).

A2 Proposal sample generation

At each step proposals were generated for all parameters by drawing from a proposal distribution centered around the current sample. Since the decomposition rates (k_i) and transport rates (B, I_m and v) have a theoretical lower bound at zero, the random walk for these parameters was performed in log-transformed space:

$$\theta' = \ln(\theta), \tag{A3a}$$

$$\theta = \exp(\theta'), \tag{A3b}$$

where θ' is the transformed parameter value and θ is the untransformed parameter value used as input for SOMPROF. In this way proposals below zero are avoided and the step become smaller when the untransformed parameters approach zero.

The conversion fractions ($\alpha_{i \to j}$) are bounded at 0 and 1, hence for these parameters the random walk was performed in logit-transformed space:

$$\theta' = \ln\left(\frac{\theta}{1-\theta}\right), \tag{A4a}$$

$$\theta = \frac{\exp(\theta')}{1+\exp(\theta')}. \tag{A4b}$$

BGD
8, 7257–7312, 2011

Similar to the log-transformation, the logit transformation assures that no steps below zero and above one are proposed, and that the steps get progressively smaller when the chains get closer to either of these bounds.

Unless corrected, the transformations affect the distribution sampled with random walk. This effect may be removed by multiplying the the acceptance chance (Eq. A1) with the Hastings factor which, in our case, is the inverse of the Jacobian of the transformation. For a log transformation:

$$J(\theta) = \theta, \tag{A5}$$

and for a logit transformation:

$$J(\theta) = \theta - \theta^2. \tag{A6}$$

The correction factor was applied for the optimizations with weak priors (setups 1 and 2). Omitting the correction factor for a log transformation effectively transforms a normal prior in transformed space into a log-normal prior in untransformed space, and analogously for a logit transformation. The prior distributions for optimization setup 3 where constructed in this way.

The proposals in transformed space were generated by drawing from a normal distribution centered around the current sample:

$$\theta'^{,*} \sim \mathcal{N}(\theta'^{,i}, \sigma). \tag{A7}$$

The step length variance σ controls the average length of the steps and is inversely proportional to the acceptance rate of the samples. By manually adjusting σ during the optimization an acceptance rate of approximately 23 % was maintained, which is the optimal rate for Gaussian posteriors (Gelman et al., 1995).

A3 Optimization design

For each optimization first a exploratory run was performed, intended to search for different posterior modes (cases). For this run, 20 chains were run in parallel, with

BGD
8, 7257–7312, 2011

starting points widely dispersed in the sampling region using Latin hypercube sampling. Furthermore, the posterior cost was reduced using a cost-reduction factor of 0.1, multiplied with the cost in Eq. (7). This effectively "flattens" the posterior, allowing the chains to escape from local modes and to take bigger steps, and thus cover more area. After all modes of interest were identified in the exploratory run, secondary runs without cost reduction were performed, where at least 4 chains were started near each mode.

The convergence of the chains was evaluated using the convergence index introduced by Gelman et al. (1995, ch. 11), which is proportional to the ratio of the between-chain variance and the within-chain variance. When the different chains converge on the same distribution, this quantity declines to 1. All chains were run for at least 20 000 iterations per chain, or until the convergence index was ≤ 1.1 for all parameters.

After the secondary runs, the chains that had not converged were discarded (it was assured that at least 4 chains had converged per run). Additionally, a variable (but at least 10 000), number of samples was removed from the start of each chain (the burn-in). Next, the remaining chains for each mode were merged and thinned to 10 000 samples for analysis by selecting samples in regular intervals.

Supplementary material related to this article is available online at: http://www.biogeosciences-discuss.net/8/7257/2011/bgd-8-7257-2011-supplement.pdf.

Acknowledgements. We thank Jim Kaste and Ryoko Fujiyoshi for providing the $^{210}Pb_{ex}$ data used in the optimizations, and Wilma Jans, Jan Elbers and Enrico Weber for supplying data for Loobos. Finally, we are grateful to Peter Buurman for giving critical comments on the optimization results and behavior Pb in soils. This work was supported by the ERC starting grant QUASOM (ERC-2007-StG-208516).

The service charges for this open access publication have been covered by the Max Planck Society.

BGD
8, 7257–7312, 2011

References

Appleby, P. G. and Oldfield, F.: The calculation of lead-210 dates assuming a constant rate of supply of unsupported ^{210}Pb to the sediment, Catena, 5, 1–8, 1978. 7265

Baisden, W. T., Amundson, R., Brenner, D. L., Cook, A. C., Kendall, C., and Harden, J. W.: A multiisotope C and N modeling analysis of soil organic matter turnover and transport as a function of soil depth in a California annual grassland soil chronosequence, Global Biogeochem. Cy., 16, 1135, doi:10.1029/2001GB001823, 2002. 7261

Beven, K. and Freer, J.: Equifinality, data assimilation, and uncertainty estimation in mechanistic modelling of complex environmental systems using the GLUE methodology, J. Hydrol., 249, 11–29, 2001. 7260

Bormann, F. and Likens, G.: Pattern and process in a forested ecosystem: disturbance, development, and the steady state based on the Hubbard Brook ecosystem study, Springer-Verlag, 1994. 7269

Boudreau, B. P.: Mathematics of tracer mixing in sediments; I, Spatially-dependent, diffusive mixing, Am. J. Sci., 286, 161–198, 1986. 7260

Braakhekke, M. C., Beer, C., Hoosbeek, M. R., Reichstein, M., Kruijt, B., Schrumpf, M., and Kabat, P.: SOMPROF: A vertically explicit soil organic matter model, Ecol. Model., 222, 1712–1730, 2011. 7259, 7260, 7261, 7262, 7263, 7268, 7272, 7279

Buurman, P. and Jongmans, A. G.: Podzolisation and soil organic matter dynamics, Geoderma, 125, 71–83, 2005. 7282

Cesarz, S., Fahrenholz, N., Migge-Kleian, S., Platner, C., and Schaefer, M.: Earthworm communities in relation to tree diversity in a deciduous forest, Eur. J. Soil Biol., 43, S61–S67, 2007. 7268

de Bruijn, A. M. G. and Butterbach-Bahl, K.: Linking carbon and nitrogen mineralization with microbial responses to substrate availability – the DECONIT model, Plant Soil, 328, 271–290, 2010. 7271

Dörr, H. and Münnich, K. O.: Downward Movement of soil organic matter and its influence on trace-element transport (^{210}Pb, ^{137}Cs) in the soil, Radiocarbon, 31, 655–663, 1989. 7261, 7283

Dörr, H. and Münnich, K. O.: Lead and cesium transport in european forest soils, Water Air Soil Poll., 57-8, 809–818, 1991. 7261

Elzein, A. and Balesdent, J.: Mechanistic Simulation of Vertical Distribution of Carbon

BGD
8, 7257–7312, 2011

Concentrations and Residence Times in Soils, Soil Sci. Soc. Am. J., 59, 1328–1335, 1995. 7261
Emmer, I. M.: Humus form and soil development during a primary succession of monoculture Pinus sylvestris on poor sandy soils, Ph.D. thesis, University of Amsterdam, Amsterdam, 1995. 7266, 7267
Eusterhues, K., Rumpel, C., Kleber, M., and Kögel-Knabner, I.: Stabilisation of soil organic matter by interactions with minerals as revealed by mineral dissolution and oxidative degradation, Org. Geochem., 34, 1591–1600, 2003. 7282
Fox, A., Williams, M., Richardson, A. D., Cameron, D., Gove, J. H., Quaife, T., Ricciuto, D., Reichstein, M., Tomelleri, E., Trudinger, C. M., and Van Wijk, M. T.: The REFLEX project: Comparing different algorithms and implementations for the inversion of a terrestrial ecosystem model against eddy covariance data, Agr. Forest Meteorol., 149, 1597–1615, 2009. 7271
Freier, K. P., Glaser, B., and Zech, W.: Mathematical modeling of soil carbon turnover in natural Podocarpus forest and Eucalyptus plantation in Ethiopia using compound specific delta ^{13}C analysis, Glob. Change Biol., 16, 1487–1502, 2010. 7261
Friedland, A. J., Craig, B. W., Miller, E. K., Herrick, G. T., Siccama, T. G., and Johnson, A. H.: Decreasing lead levels in the forest floor of the northeastern USA, Ambio, 21, 400–403, 1992. 7284
Fujiyoshi, R. and Sawamura, S.: Mesoscale variability of vertical profiles of environmental radionuclides (K-40, Ra-226, Pb-210 and Cs-137) in temperate forest soils in Germany, Sci. Total Environ., 320, 177–188, 2004. 7269
Gelman, A., Carlin, J. B., Stern, S., and Rubin, D. B.: Bayesian data analysis, Chapman & Hall, 1995. 7270, 7287, 7288
Golchin, A., Oades, J. M., Skjemstad, J. O., and Clarke, P.: Soil-structure and carbon cycling, Aust. J. Soil Res., 32, 1043–1068, 1994. 7279
Hastings, W. K.: Monte-Carlo sampling methods using Markov chains and their applications, Biometrika, 57, 97–109, 1970. 7285
He, Q. and Walling, D. E.: The distribution of fallout Cs-137 and Pb-210 in undisturbed and cultivated soils, Appl. Radiat. Isotopes, 48, 677–690, 1997. 7261
Heimann, M. and Reichstein, M.: Terrestrial ecosystem carbon dynamics and climate feedbacks, Nature, 451, 289–292, 2008. 7259
IUSS Working Group WRB: World Reference Base for Soil Resources 2006, first update 2007,

BGD
8, 7257–7312, 2011

Tech. rep., FAO, 2007. 7266, 7268
Jenkinson, D. S. and Coleman, K.: The turnover of organic carbon in subsoils. Part 2. Modelling carbon turnover, Eur. J. Soil Sci., 59, 400–413, 2008. 7259
Jobbagy, E. G. and Jackson, R. B.: The vertical distribution of soil organic carbon and its relation to climate and vegetation, Ecol. Appl., 10, 423–436, 2000. 7282
Kaiser, K. and Guggenberger, G.: The role of DOM sorption to mineral surfaces in the preservation of organic matter in soils, Org. Geochem., 31, 711–725, 2000. 7260
Kalbitz, K. and Kaiser, K.: Contribution of dissolved organic matter to carbon storage in forest mineral soils, J. Plant Nutr. Soil Sc., 171, 52–60, 2008. 7282
Kaste, J. M., Friedland, A. J., and Sturup, S.: Using stable and radioactive isotopes to trace atmospherically deposited Pb in montane forest soils, Environ. Sci. Technol., 37, 3560–3567, 2003. 7283
Kaste, J. M., Heimsath, A. M., and Bostick, B. C.: Short-term soil mixing quantified with fallout radionuclides, Geology, 35, 243–246, 2007. 7261, 7269, 7300
Kindler, R., Siemens, J., Kaiser, K., Walmsley, D. C., Bernhofer, C., Buchmann, N., Cellier, P., Eugster, W., Gleixner, G., Grunwald, T., Heim, A., Ibrom, A., Jones, S. K., Jones, M., Klumpp, K., Kutsch, W., Larsen, K. S., Lehuger, S., Loubet, B., McKenzie, R., Moors, E., Osborne, B., Pilegaard, K., Rebmann, C., Saunders, M., Schmidt, M. W. I., Schrumpf, M., Seyfferth, J., Skiba, U., Soussana, J. F., Sutton, M. A., Tefs, C., Vowinckel, B., Zeeman, M. J., and Kaupenjohann, M.: Dissolved carbon leaching from soil is a crucial component of the net ecosystem carbon balance, Glob. Change Biol., 17, 1167–1185, 2011. 7278, 7279, 7306, 7311
Knorr, W. and Kattge, J.: Inversion of terrestrial ecosystem model parameter values against eddy covariance measurements by Monte Carlo sampling, Glob. Change Biol., 11, 1333–1351, 2005. 7286
Kögel-Knabner, I., Guggenberger, G., Kleber, M., Kandeler, E., Kalbitz, K., Scheu, S., Eusterhues, K., and Leinweber, P.: Organo-mineral associations in temperate soils: Integrating biology, mineralogy, and organic matter chemistry, J. Plant Nutr. Soil Sc., 171, 61–82, 2008. 7282
Koven, C., Friedlingstein, P., Ciais, P., Khvorostyanov, D., Krinner, G., and Tarnocai, C.: On the formation of high-latitude soil carbon stocks: Effects of cryoturbation and insulation by organic matter in a land surface model, Geophys. Res. Lett., 36, L21501, doi:10.1029/2009GL040150, 2009. 7259

BGD
8, 7257–7312, 2011

Kutsch, W., Persson, T., Schrumpf, M., Moyano, F., Mund, M., Andersson, S., and Schulze, E.-D.: Heterotrophic soil respiration and soil carbon dynamics in the deciduous Hainich forest obtained by three approaches, Biogeochemistry, 100, 1–17, 2010. 7267, 7268, 7269, 7296
Kylander, M. E., Cortizas, A. M., Rauch, S., and Weiss, D. J.: Lead penetration and leaching in a complex temperate soil profile, Environ. Sci. Technol., 42, 3177–3184, 2008. 7283
Lloyd, J. and Taylor, J. A.: On the Temperature Dependence of Soil Respiration, Funct. Ecol., 8, 315–323, 1994. 7296
Logan, E. M., Pulford, I. D., Cook, G. T., and MacKenzie, A. B.: Complexation of Cu2+ and Pb2+ by peat and humic acid, Eur. J. Soil Sci., 48, 685–696, 1997. 7283, 7284
Mabit, L., Klik, A., Benmansour, M., Toloza, A., Geisler, A., and Gerstmann, U. C.: Assessment of erosion and deposition rates within an Austrian agricultural watershed by combining Cs-137, Pb-210(ex) and conventional measurements, Geoderma, 150, 231–239, 2009. 7261
Mead, R.: A generalised logit-normal distribution, Biometrics, 21, 721–732, 1965. 7272
Metropolis, N., Rosenbluth, A. W., Rosenbluth, M. N., Teller, A. H., and Teller, E.: Equation of state calculations by fast computing machines, J. Chem. Phys., 21, 1087–1092, 1953. 7285
Michalzik, B., Kalbitz, K., Park, J. H., Solinger, S., and Matzner, E.: Fluxes and concentrations of dissolved organic carbon and nitrogen – a synthesis for temperate forests, Biogeochemistry, 52, 173–205, 2001. 7278
Mikutta, R., Kleber, M., Torn, M. S., and Jahn, R.: Stabilization of soil organic matter: Association with minerals or chemical recalcitrance?, Biogeochemistry, 77, 25–56, 2006. 7282
Miller, E. K. and Friedland, A. J.: Lead migration in forest soils - response to changing atmospheric inputs, Environ. Sci. Technol., 28, 662–669, 1994. 7284
Mosegaard, K. and Sambridge, M.: Monte Carlo analysis of inverse problems, Inverse Probl., 18, R29–R54, 2002. 7270
Mosegaard, K. and Tarantola, A.: Monte Carlo sampling of solutions to inverse problems, J. Geophys. Res.-Sol. Ea., 100, 12431–12447, 1995. 7286
Nierop, K. G. J.: Origin of aliphatic compounds in a forest soil, Org. Geochem., 29, 1009–1016, 1998. 7282
Nierop, K. G. J. and Buurman, P.: Water-soluble organic matter in incipient podzols: accumulation in B horizons or in fibres?, Eur. J. Soil Sci., 50, 701–711, 1999. 7282
Parton, W. J., Schimel, D. S., Cole, C. V., and Ojima, D. S.: Analysis of Factors Controlling Soil Organic Matter Levels in Great Plains Grasslands, Soil Sci. Soc. Am. J., 51, 1173–1179, 1987. 7259

BGD
8, 7257–7312, 2011

Rasse, D. P., Rumpel, C., and Dignac, M.-F.: Is soil carbon mostly root carbon? Mechanisms for a specific stabilisation, Plant Soil, 269, 341–356, 2005. 7260, 7282
Reichstein, M. and Beer, C.: Soil respiration across scales: The importance of a model-data integration framework for data interpretation, J. Plant Nutr. Soil Sc., 171, 344–354, 2008. 7259
Rumpel, C. and Kögel-Knabner, I.: Deep soil organic matter-a key but poorly understood component of terrestrial C cycle, Plant Soil, 338, 143–158, 2011. 7259
Rumpel, C., Kögel-Knabner, I., and Bruhn, F.: Vertical distribution, age, and chemical composition of organic, carbon in two forest soils of different pedogenesis, Org. Geochem., 33, 1131–1142, 2002. 7259
Salomé, C., Nunan, N., Pouteau, V., Lerch, T. Z., and Chenu, C.: Carbon dynamics in topsoil and in subsoil may be controlled by different regulatory mechanisms, Glob. Change Biol., 16, 416–426, 2010. 7259
Sauve, S., Martinez, C. E., McBride, M., and Hendershot, W.: Adsorption of free lead (Pb2+) by pedogenic oxides, ferrihydrite, and leaf compost, Soil Sci. Soc. Am. J., 64, 595–599, 2000. 7283
Scharnagl, B., Vrugt, J. A., Vereecken, H., and Herbst, M.: Information content of incubation experiments for inverse estimation of pools in the Rothamsted carbon model: a Bayesian perspective, Biogeosciences, 7, 763–776, doi:10.5194/bg-7-763-2010, 2010. 7271
Schimel, D. S., Braswell, B. H., Holland, E. A., McKeown, R., Ojima, D. S., Painter, T. H., Parton, W. J., and Townsend, A. R.: Climatic, edaphic, and biotic controls over storage and turnover of carbon in soils, Global Biogeochem. Cy., 8, 279–293, 1994. 7259
Schroth, A. W., Bostick, B. C., Kaste, J. M., and Friedland, A. J.: Lead sequestration and species redistribution during soil organic matter decomposition, Environ. Sci.Technol., 42, 3627–3633, 2008. 7283
Schrumpf, M., Schulze, E. D., Kaiser, K., and Schumacher, J.: How accurately can soil organic carbon stocks and stock changes be quantified by soil inventories?, Biogeosciences, 8, 1193–1212, doi:10.5194/bg-8-1193-2011, 2011. 7269
Smit, A.: The impact of grazing on spatial variability of humus profile properties in a grass-encroached Scots pine ecosystem, Cate, 36, 85–98, 1999. 7266
Smit, A. and Heuvelink, G. B. M.: Exploring the use of sequential sampling for monitoring organic matter stocks in a grazed and non-grazed Scots pine stand, Geoderma, 139, 118–126, 2007. 7296

BGD
8, 7257–7312, 2011

Smit, A. and Kooijman, A. M.: Impact of grazing on the input of organic matter and nutrients to the soil in a grass-encroached Scots pine forest, For. Ecol. Manage., 142, 99–107, 2001. 7296
Tonneijck, F. H. and Jongmans, A. G.: The influence of bioturbation on the vertical distribution of soil organic matter in volcanic ash soils: a case study in northern Ecuador, Eur. J. Soil Sci., 59, 1063–1075, 2008. 7260
Trumbore, S.: Radiocarbon and Soil Carbon Dynamics, Annu. Rev. Earth Pl. Sc., 37, 47–66, 2009. 7259
Turner, D. R., Varney, M. S., Whitfield, M., Mantoura, R. F. C., and Riley, J. P.: Electrochemical studies of copper and lead complexation by fulvic-acid. 1. potentiometric measurements and a critical comparison of metal-binding models, Geochim. Cosmochim. Ac., 50, 289–297, 1986. 7284
Urban, N. R., Eisenreich, S. J., Grigal, D. F., and Schurr, K. T.: Mobility and diagenesis of Pb and Pb-210 in peat, Geochim. Cosmochim. Ac., 54, 3329–3346, 1990. 7284
Veresoglou, D. S. and Fitter, A. H.: Spatial and temporal patterns of growth and nutrient-uptake of 5 co-existing grasses, J. Ecol., 72, 259–272, 1984. 7267
von Lützow, M., Kögel-Knabner, I., Ekschmitt, K., Matzner, E., Guggenberger, G., Marschner, B., and Flessa, H.: Stabilization of organic matter in temperate soils: mechanisms and their relevance under different soil conditions – a review, Eur. J. Soil Sci., 57, 426–445, 2006. 7259
Wakiyama, Y., Onda, Y., Mizugaki, S., Asai, H., and Hiramatsu, S.: Soil erosion rates on forested mountain hillslopes estimated using Cs-137 and Pb-210(ex), Geoderma, 159, 39–52, 2010. 7261
Walling, D. E. and He, Q.: Using fallout lead-210 measurements to estimate soil erosion on cultivated land, Soil Sci. Soc. Am. J., 63, 1404–1412, 1999. 7261
Wang, E. X. and Benoit, G.: Fate and transport of contaminant lead in spodosols: A simple box model analysis, Water Air Soil Poll., 95, 381–397, 1997. 7284
WUR, Alterra: Loobos site, http://www.climatexchange.nl/sites/loobos/index.htm, access: 8 March 2011. 7266
Yeluripati, J. B., van Oijen, M., Wattenbach, M., Neftel, A., Ammann, A., Parton, W. J., and Smith, P.: Bayesian calibration as a tool for initialising the carbon pools of dynamic soil models, Soil Biol. Biochem., 41, 2579–2583, 2009. 7271

BGD
8, 7257–7312, 2011

Yoo, K., Ji, J. L., Aufdenkampe, A., and Klaminder, J.: Rates of soil mixing and associated carbon fluxes in a forest versus tilled agricultural field: Implications for modeling the soil carbon cycle, J. Geophys. Res.-Biogeo., 116, G01014, doi:10.1029/2010JG001304, 2011. 7261

BGD
8, 7257–7312, 2011

Table 1. Model driving data and not-optimized parameters.

Variable/Parameter	Loobos	Hainich	Units
Annual above ground litter input	0.310	0.314[1]	kgC m^{-2} yr^{-1}
From canopy	0.255	0.277	
From understory	0.055[2]	0.037	
Total annual root litter input	0.445	0.178[1]	kgC m^{-2} yr^{-1}
From canopy	0.02[3]	0.148	
From understory	0.425[2]	0.03	
Root litter distribution parameter	0.4	0.07	m^{-1}
Soil temperature response parameter	308.56[4]	308.56[4]	K
Soil moisture response parameter a[5]	1	1	–
Soil moisture response parameter b[5]	20	20	–
Soil temperature	*	*	K
Relative soil moisture content	*	*	–
Bulk density L layer	50	50	kg m^{-3}
Bulk density F layer	100	100	kg m^{-3}
Bulk density H layer	150	150	kg m^{-3}
Bulk density mineral soil	1400	*	kg m^{-3}
Simulation period	95	1000	yr
Depth of bottom boundary	2	0.7	m

* Variable in depth and/or time.
[1] Kutsch et al. (2010); W. Kutsch (personal communication, 2009) .
[2] Smit and Kooijman (2001).
[3] Smit and Heuvelink (2007).
[4] Lloyd and Taylor (1994).
[5] Soil moisture response function: $g(W) = \exp(-\exp(a - bW))$.

BGD
8, 7257–7312, 2011

Table 2. Optimized model parameters.

Parameter	Symbol	Units	Prior distribution	Upper bound
Decomposition rates at 10 °C and optimal soil moisture				
Above ground litter	k_{AGL}	yr^{-1}	Log–$\mathcal{N}(-0.81, 0.76)$	3
Root litter	k_{RL}	yr^{-1}	Log–$\mathcal{N}(-0.81, 0.76)$	3
Fragmented litter	k_{FL}	yr^{-1}	Log–$\mathcal{N}(-0.81, 0.76)$	3
Non-leachable slow organic matter	k_{NLS}	yr^{-1}	Log–$\mathcal{N}(-3.25, 1.05)$	3
Leachable slow organic matter	k_{LS}	yr^{-1}	Log–$\mathcal{N}(-3.25, 1.05)$	3
Transformation factors				
Aboveground litter-fragmented litter	$\alpha_{AGL \to FL}$	–	Logit–$\mathcal{N}((0.70, 1.20)$	1
Fragmented litter-NLS-OM	$\alpha_{FL \to NLS}$	–	Logit–$\mathcal{N}(-1.50, 1.20)$	$1, (1 - \alpha_{FL \to LS})$
Fragmented litter-LS-OM	$\alpha_{FL \to LS}$	–	Logit–$\mathcal{N}(-1.50, 1.20)$	$1, (1 - \alpha_{FL \to NLS})$
Root litter-NLS-OM	$\alpha_{RL \to NLS}$	–	Logit–$\mathcal{N}(-1.50, 1.20)$	$1, (1 - \alpha_{RL \to LS})$
Root litter-LS-OM	$\alpha_{RL \to LS}$	–	Logit–$\mathcal{N}(-1.50, 1.20)$	$1, (1 - \alpha_{RL \to NLS})$
Transport parameters				
Bioturbation rate	B	$kg\,m^{-2}\,yr^{-1}$	–	3
Mixing length	l_m	m	–	3
Advection rate	v	$mm\,yr^{-1}$	–	3

BGD
8, 7257–7312, 2011

Table 3. Minimum cost for each of the posterior cases (see also Supplement Figs. 2 and 5).

Optimization	Minimum cost	
	Loobos	Hainich
1: Excl. $^{210}Pb_{ex}$; weak priors	A: 189.02 B: 152.25	A: 226.97 B: 223.24 C: 221.88
2: Incl. $^{210}Pb_{ex}$; weak priors	A: 891.08 B: 155.90	A: 228.77 B: 229.99 C: 243.40
3: Incl. $^{210}Pb_{ex}$; strong priors	169.91	A: 251.90 B: 248.54 C: 272.15

BGD
8, 7257–7312, 2011

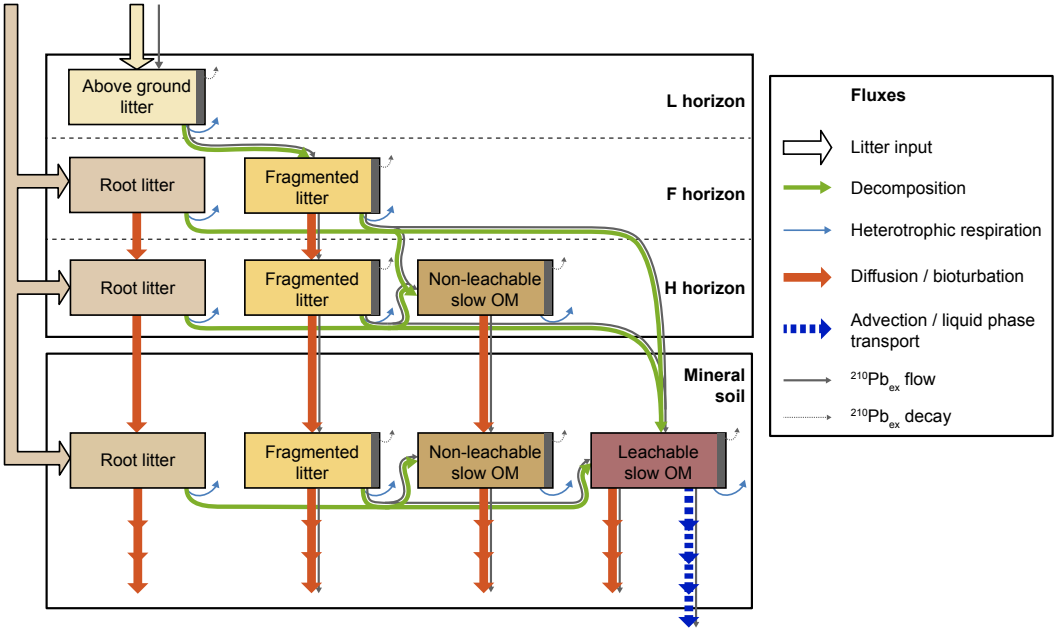

Fig. 1. Overview of the SOMPROF model and the $^{210}Pb_{ex}$ module. The dark gray rectangles indicate $^{210}Pb_{ex}$ associated with the organic matter pools.

BGD
8, 7257–7312, 2011

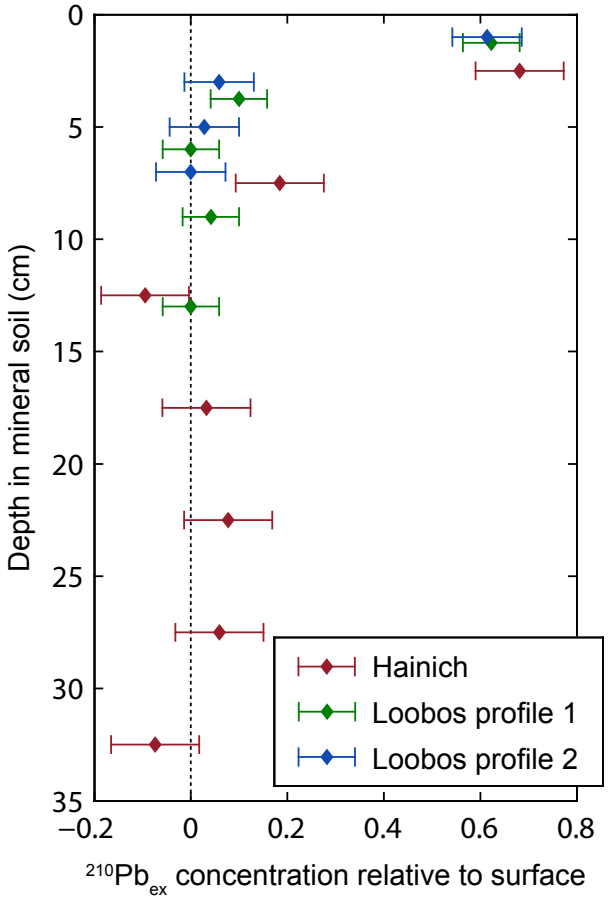

Fig. 2. Measured $^{210}Pb_{ex}$ concentrations used for the optimization. Concentrations are relative to the values at the surface. Note that the $^{210}Pb_{ex}$ measurements for Loobos are taken from an equivalent site (Kaste et al., 2007).

BGD
8, 7257–7312, 2011

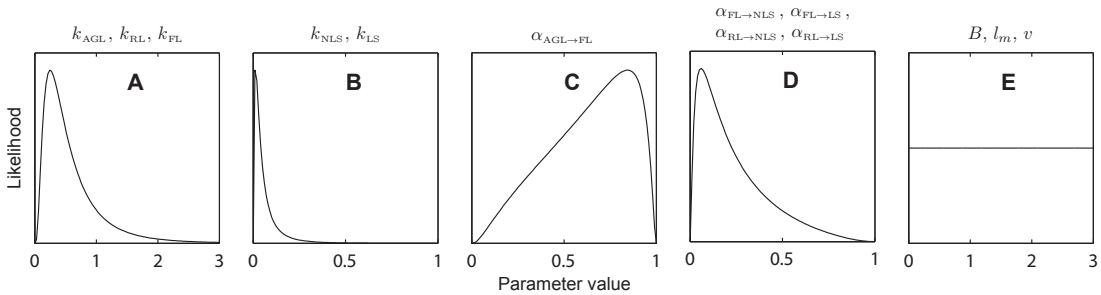

Fig. 3. Prior distributions used for the model parameters. Distributions: **(A)**: Log–$\mathcal{N}(-0.81, 0.76)$; **(B)**: Log–$\mathcal{N}(-3.25, 1.05)$; **(C)**: Logit–$\mathcal{N}(0.70, 1.20$; **(D)**: Logit–$\mathcal{N}(-1.50, 1.20)$; **(E)**: uniform prior.

BGD
8, 7257–7312, 2011

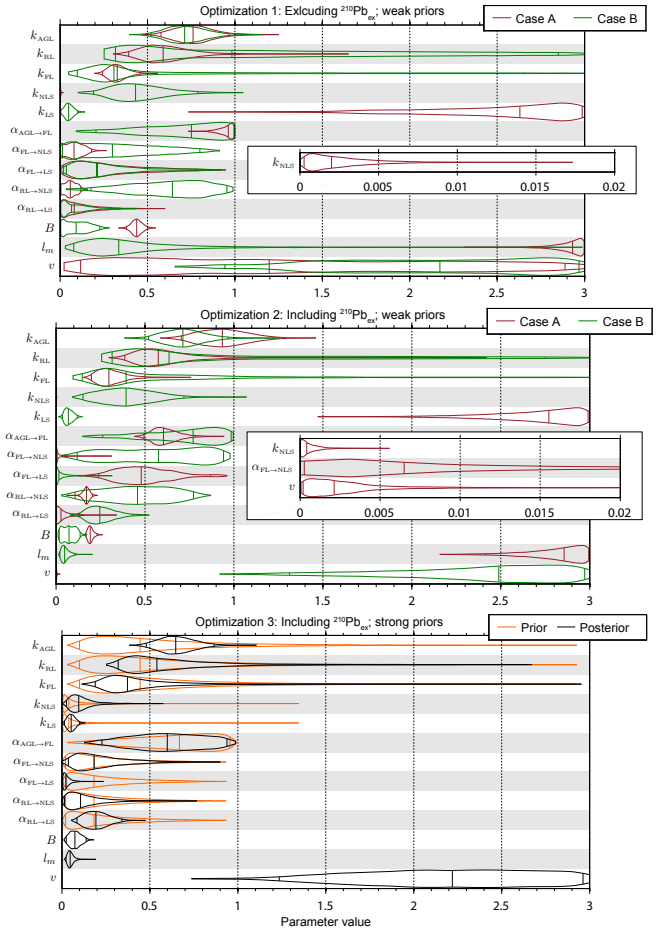

Fig. 4. Violin plots of the optimization results for Loobos. For optimizations 1 and 2, two cases (posterior modes) are shown; see text for further explanation. For optimization 3, the graph shows the prior and posterior distributions. The violins indicate the marginal distributions for each parameter. The three vertical lines inside the violins indicate the median and the 95 % confidence bounds.

BGD
8, 7257–7312, 2011

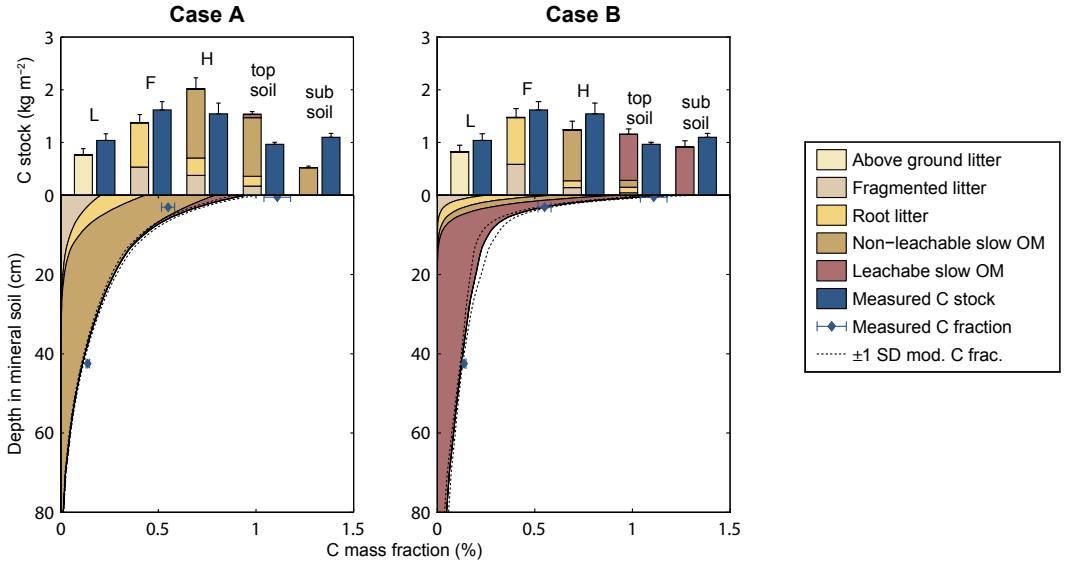

Fig. 5. Measured and modeled carbon stocks (topsoil: 0–30 cm; subsoil: >30 cm) and mass fractions for Loobos. Model results are from forward Monte Carlo runs based on posterior samples from the two cases of optimization setup 1 (excluding $^{210}Pb_{ex}$ and with weak priors). Depicted stocks and fractions are averages. Errorbars denote one standard error of the mean for the measurements and one standard deviation for the model results.

BGD
8, 7257–7312, 2011

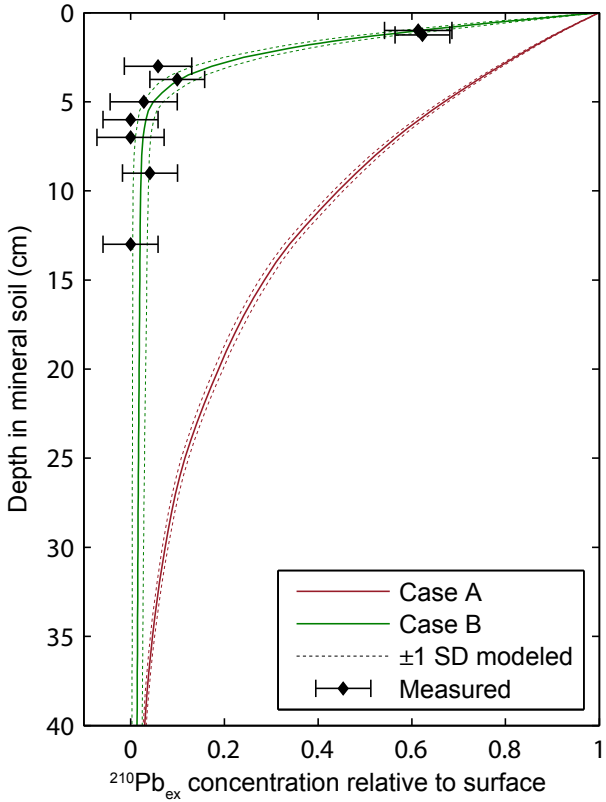

Fig. 6. Measured and modeled $^{210}Pb_{ex}$ profile for Loobos. Modeled results are from forward Monte Carlo runs based on posterior samples from the two cases of optimization setup 2 (including $^{210}Pb_{ex}$ and with weak priors).

BGD
8, 7257–7312, 2011

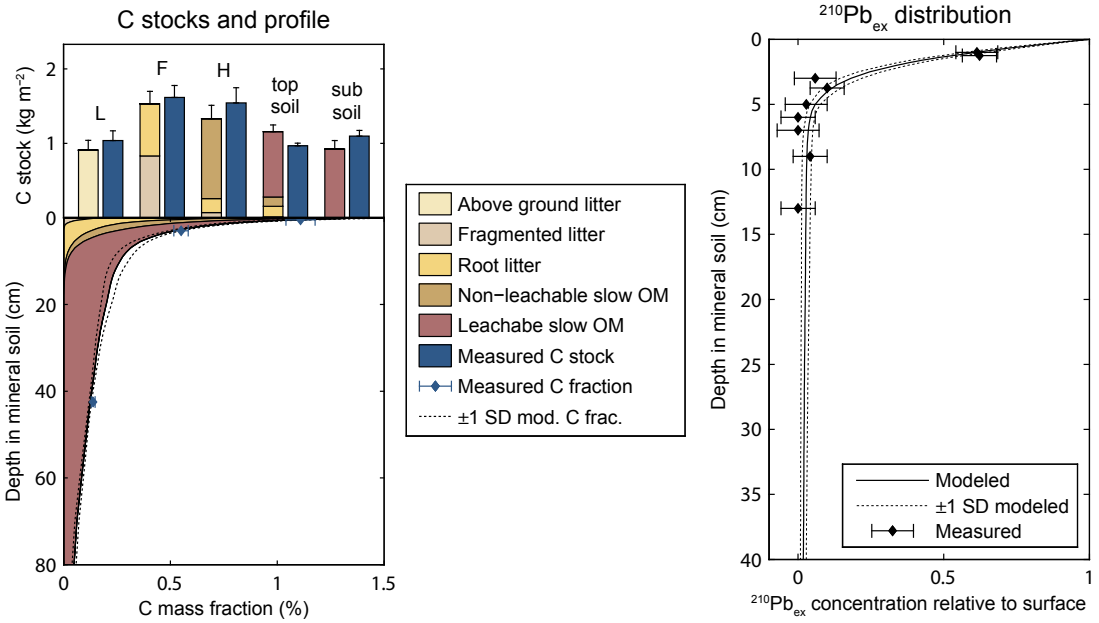

Fig. 7. Results from the forward Monte Carlo runs for Loobos using posterior samples from the optimization setup 3 (including ^{210}Pb$_{ex}$ and with strong priors). Errorbars indicate one standard error of the mean for the measurements and one standard deviation for the model results. (topsoil: 0–30 cm; subsoil: >30 cm).

BGD
8, 7257–7312, 2011

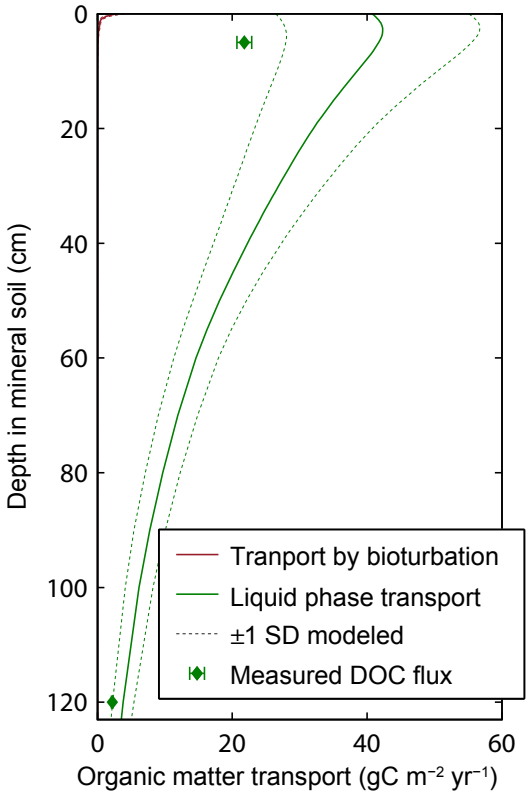

Fig. 8. Modeled vertical transport fluxes for Loobos, from forward Monte Carlo simulations based on posterior samples of optimization setup 3 (including $^{210}Pb_{ex}$ and with strong priors). The depicted fluxes are averages for the last simulation year. The dashed line indicates the standard deviation over the Monte Carlo ensemble. Measured DOC fluxes were taken from Kindler et al. (2011). Note the somewhat indistinct bioturbation flux in the upper left corner.

BGD
8, 7257–7312, 2011

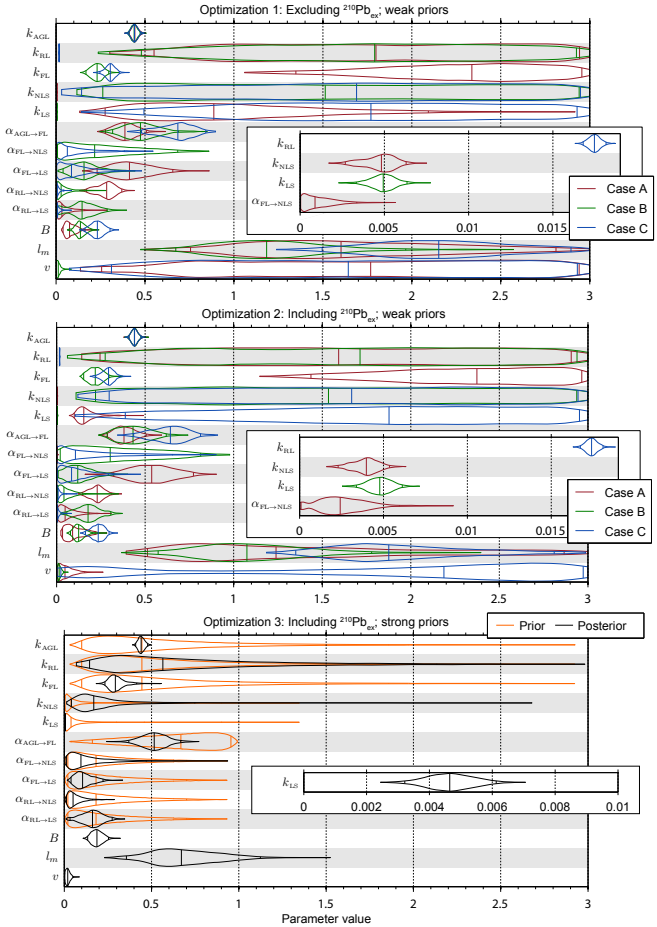

Fig. 9. Violin plots of the optimization results for Hainich. For optimizations 1 and 2, three cases (posterior modes) are shown; see text for further explanation. For optimization 3, the graph shows the prior distribution and most likely case of the posterior distribution. The violins indicate the marginal distributions for each parameter. The three vertical lines inside the violins indicate the median and the 95 % confidence bounds.

BGD
8, 7257–7312, 2011

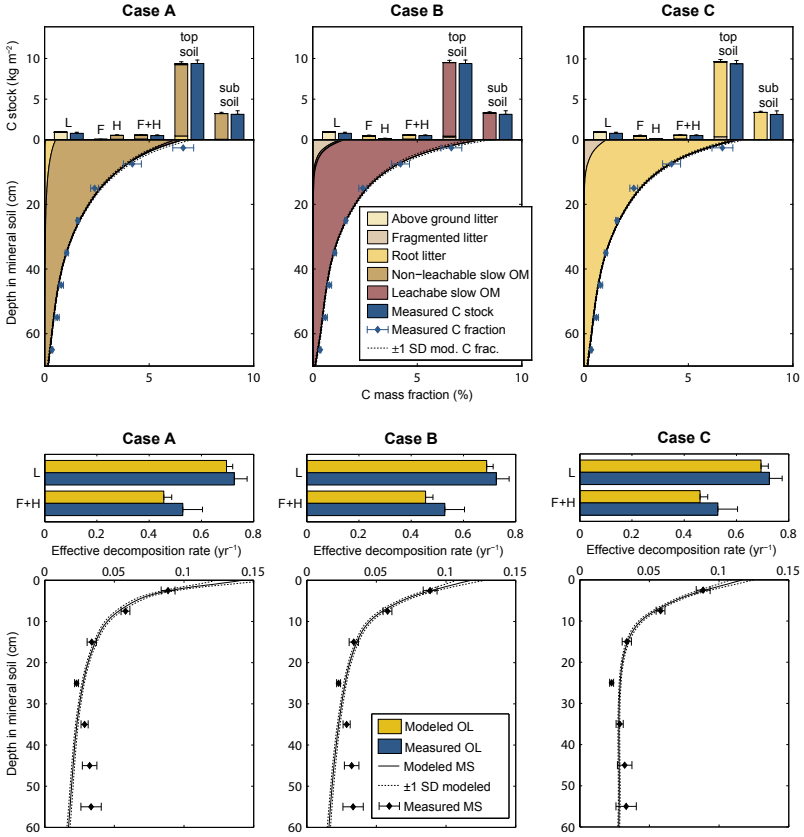

Fig. 10. Results from forward Monte Carlo simulations for Hainich based on posterior samples from the three cases of optimization 1 (excluding $^{210}Pb_{ex}$ and with weak priors). Top: measured and modeled carbon stocks (topsoil: 0–30 cm; subsoil: >30 cm) and mass fractions; bottom: measured and modeled effective decomposition rates. All depicted values are averages. Errorbars denote one standard error of the mean for the measurements and one standard deviation for the model results.

BGD
8, 7257–7312, 2011

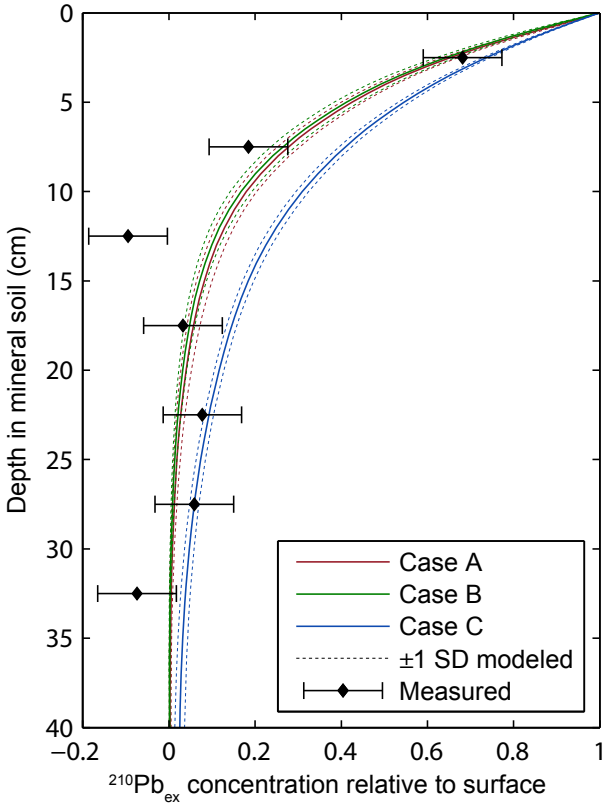

Fig. 11. Measured and modeled $^{210}Pb_{ex}$ profile for Hainich. Modeled results are from forward Monte Carlo runs based on posterior samples from the three cases of optimization setup 2 (including $^{210}Pb_{ex}$ and with weak priors).

BGD
8, 7257–7312, 2011

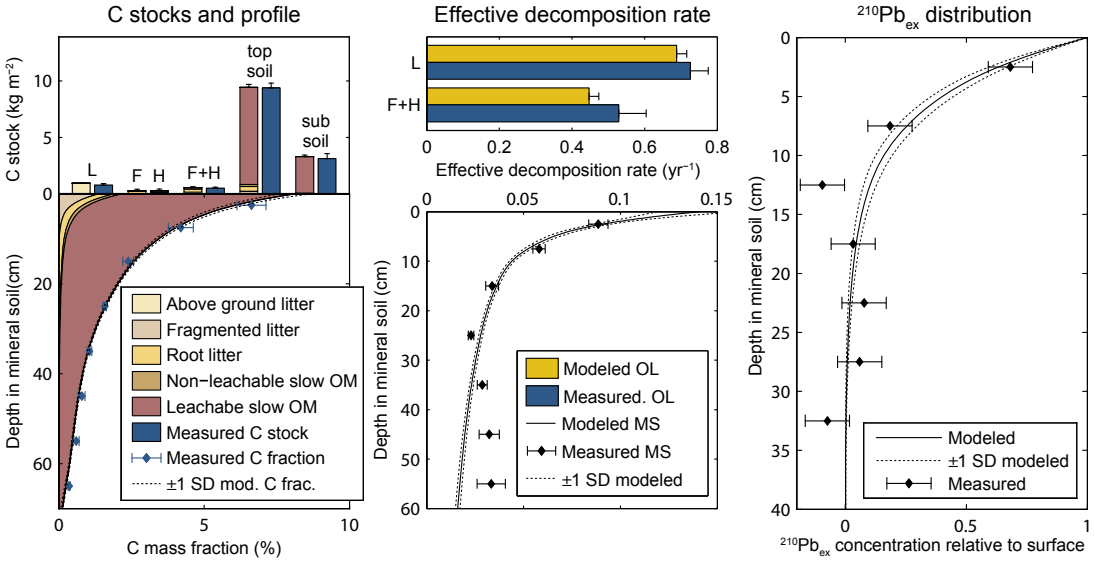

Fig. 12. Results from the forward Monte Carlo runs for Hainich using posterior samples from the most likely case (B) of the optimization setup 3 (including $^{210}Pb_{ex}$ and with strong priors). Errorbars indicate one standard error of the mean for the measurements and one standard deviation for the model results (topsoil: 0–30 cm; subsoil: >30 cm).

BGD
8, 7257–7312, 2011

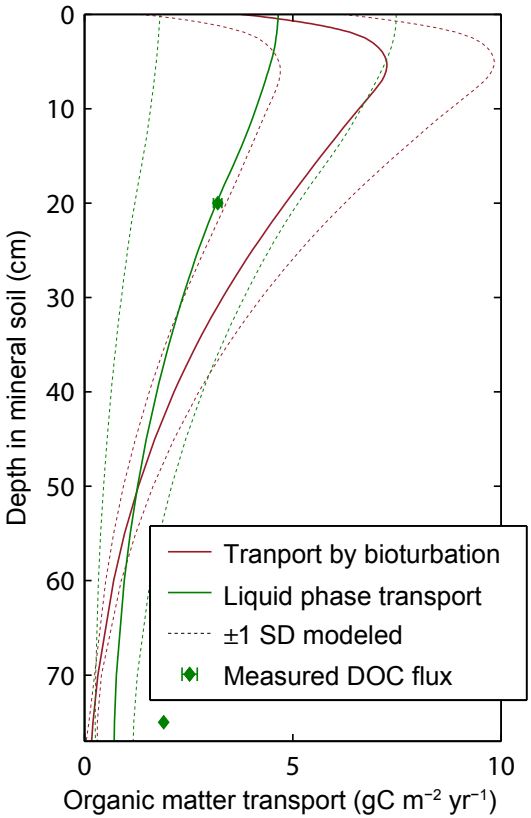

Fig. 13. Modeled vertical transport fluxes for Hainich, from forward Monte Carlo simulations based on posterior samples of the most likely case case (B) of optimization setup 3. The depicted fluxes are averages for the last simulation year. The dashed lines indicate the standard deviation over the Monte Carlo ensemble. Measured DOC fluxes were taken from Kindler et al. (2011).

BGD
8, 7257–7312, 2011

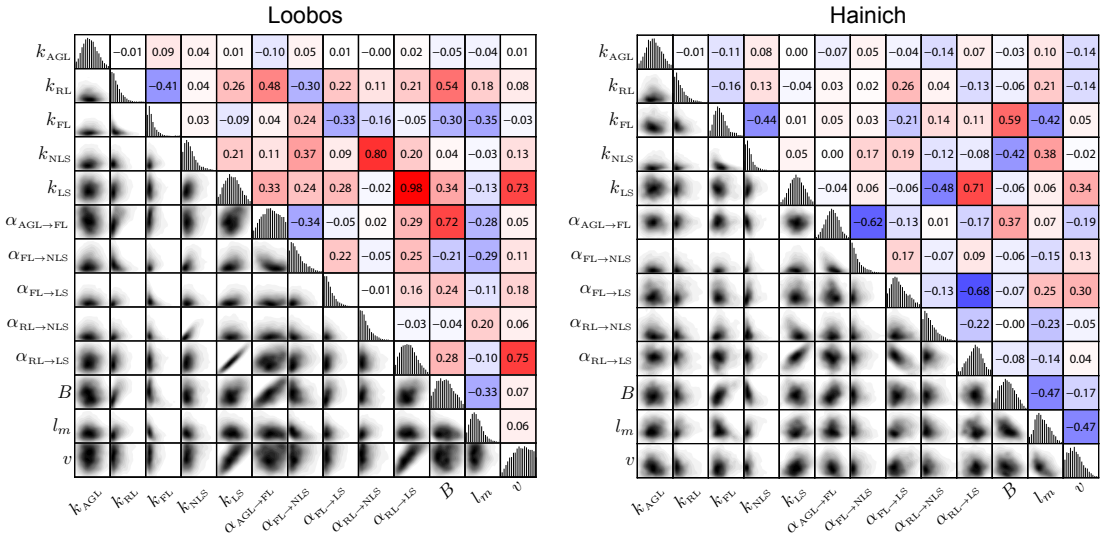

Fig. 14. Correlation matrix of the posterior sample for optimization 3 (including $^{210}Pb_{ex}$ and with strong priors) for Loobos and Hainich (case B). The figure shows the correlations for each possible combination of two parameters. In the lower triangle bivariate density probability plots are depicted. In the upper triangle the correlation coefficients are shown, with blue indicating negative correlations and red positive correlations. On the diagonal histograms of the univariate marginal distribution for each parameter are shown.

BGD
8, 7257–7312, 2011

Modeling the SOM profile using $^{210}Pb_{ex}$ measurements and Bayesian inversion

M. C. Braakhekke et al.